# Analytical Model of Satellite Based Entanglement Distribution

Janice van Dam
5405777

March 2022

TU Delft

# Thesis report

on

# Analytical Modelling of Satellite Based Entanglement Distribution

by

Janice van Dam

to obtain the degree of Master of Science at the Delft University of Technology,
to be defended publicly on Wednesday March 16th, 2022.


| | |
|---|---|
| Student number: | 5405777 |
| Institution: | Delft University of Technology |
| Place: | Faculty of Applied Sciences, Delft |
| Project Duration: | July, 2021 - March, 2022 |
| Daily supervision: | D. Maier, Msc. |
| Thesis committee: | Prof. dr. S. D. C. Wehner,<br>Assistant Prof. dr. J. Borregaard,<br>Dr. ir. T. H. Taminiau |


# Acknowledgements

First of all I would like to thank Stephanie Wehner for being an inspiring role model and giving me the opportunity to develop myself in her group at QuTech. I also want to thank Johannes Borregaard and David Maier for the daily supervision and helping to shape the model to what it has become. All discussions have greatly helped my understanding of the field.
I would also like to acknowledge some more people that helped with discussing the model and its results. Specifically Vicky Dominguez Tubio, Raja Yehia, Matteo Schiavon and Rudolf Saathof, who helped in discussing the satellite and space parts of the model, which is not generally an area of expertise in QuTech. Also thank you to the members of the QuTech blueprint team, who were willing to discuss some weird outcomes even if they didn't really know what was going on in my project.
I want to thank my parents for believing in me, as well as the other master students at QuTech who have kept me company throughout this process. And lastly, thank you to Sander, for always pushing me to do better and listening to my complaints and victories (and for sending me memes).

**Abstract**

For a global quantum communication network, we need to have long distance links over which we can distribute entangled photon pairs. Due to exponential losses, using optical fibres alone is unfeasible. Quantum repeaters extend the range of quantum networks, but intercontinental links are still unfeasible. Because of this, research has gone towards exploring space based segments, where a satellite can be used to make long-distance links by making use of the lower losses of free space transmission compared to fibre transmission.

Here, we develop a general analytical model to compute the rate and fidelity of setups consisting of two ground stations connected by a satellite in orbit. We consider three different schemes: a direct downlink and two memory assisted schemes where the satellite is used as a quantum repeater, in an uplink and a downlink. Combining orbital mechanics for the satellite with a detailed model for transmission probability, allows us to track what happens to the rate and fidelity at any point in time. The generality of the model allows for a broad applicability, fitting to many different setups.

We apply our model to different setups by tuning the different parameters and identify that the rate of the protocol will benefit most from increasing the multimode capacity of our assisting quantum memory and that the fidelity is most benefited by a good entanglement swap in the memory assisted schemes. If we have small links, bad memories or a bad entanglement swap, the direct downlink protocol will be the best choice, but for an intercontinental link we will need our memory assisted schemes.

# Contents

# List of variables

| Variable | Meaning | Introduced in Section |
|---|---|---|
| $c_\sigma^\dagger$ | creation operator for mode c | 1.4 |
| $p_0$ | probability of creating desired Bell state | 2.1.1 |
| $p_b$ | probability of source successfully emitting two photons | 2.1.1 |
| $p_x$ | probability of emitting state x | 2.1.1 |
| $p_w$ | probability of success in photon emission | 2.1.1 |
| $\rho_\gamma$ | mixture of possible 2 photon states emitted from the source | 2.1.1 |
| $p_T$ | transmission probability | 2.1.2 |
| $p_{\text{dark, d}}$ | dark count probability, modelled as decoherence | 2.1.3 |
| $p_{\text{dark, v}}$ | dark count probability, modelled as storing vacuum | 2.1.3 |
| $\eta_h$ | heralding efficiency | 2.1.3 |
| $\eta_{c,l}(t)(\mu_{c,l}(t))$ | total memory efficiency for loss at receiver (emitter) | 2.1.4 |
| $\eta_{c,d}(t)(\mu_{c,d}(t))$ | total memory efficiency for decoherence at receiver (emitter) | 2.1.4 |
| $\tau$ | coherence time of memory | 2.1.4 |
| $\eta^X$ | fraction of times the state $X$ is detected in BSM | 2.1.5 |
| $\eta_{\text{BSM}}$ | efficiency of distinguishing states in BSM | 2.1.5 |
| $p_{\text{BSM}}$ | probability of not depolarizing in BSM | 2.1.5 |
| $h$ | height of the satellite about the earth's surface | 2.2.1 |
| $R_\oplus$ | radius Earth | 2.2.1 |
| $\theta_e$ | angular velocity of earth's rotation | 2.2.1 |
| $x, y$ | coordinates of ground station position | 2.2.1 |
| $\theta_s$ | angular velocity of satellite ($=2\pi/T$) | 2.2.1 |
| $T$ | orbital period satellite ($=2\pi\sqrt{(R_\oplus+h)^3/GM_\oplus}$) | 2.2.1 |
| $G$ | gravitational constant | 2.2.1 |
| $M_\oplus$ | mass Earth | 2.2.1 |
| $\zeta$ | zenith angle (angle between ground station's zenith and the satellite) | 2.2.1 |
| $w_0$ | beam waist of Gaussian beam | 2.2.3 |
| $I_0$ | intensity of Gaussian beam | 2.2.3 |
| $z$ | beam propagation distance | 2.2.3 |
| $w(z)$ | beam width | 2.2.3 |
| $\lambda$ | wavelength | 2.2.3 |
| $Z_0$ | Rayleigh distance ($=\frac{\pi w_0^2}{\lambda}$) | 2.2.3 |
| $T$ | additional beam spreading due to turbulance | 2.2.3 |
| $C_n^2$ | index structure constant | 2.2.3 |
| $v$ | windspeed at high altitude | 2.2.3 |
| $A$ | turbulence strength at the ground level | 2.2.3 |
| $P_R$ | received power | 2.2.3 |
| $P_E$ | emitted power | 2.2.3 |
| $L_p$ | pointing loss | 2.2.3 |
| $L_T, L_R$ | transmitter, receiver loss | 2.2.3 |
| $L_j$ | loss due to pointing jitter | 2.2.3 |
| $L_{ATM}$ | loss due to regular extinction ($=10^{-\frac{4.34\tau(0)\sec(\zeta)}{10}}$) | 2.2.3 |
| $\eta_0$ | $=L_pL_TL_RL_{ATM}L_j$ | 2.2.3 |
| $N_{\text{mem}}$ | number of memory slots | 2.3.1 |
| $r_{\text{rep}}$ | source repetition rate | 2.3.1 |
| $T_{\text{com}}$ | communication time between ground, satellite (=L/c) | 2.3.1 |
| $p_{h,c}$ | $=p_w p_{T,c}\eta_h$ | 2.3.1 |
| $t_{\text{fire}}$ | time it takes to create $N_{\text{mem}}$ photons and 'fire' them down | 2.3.2 |
| $t_{\text{attempt}}$ | time it takes to have one attempt of creating entanglement in one arm | 2.3.2 |
| $N_{\max}$ | maximum attempts before the memories reset | 2.3.2 |
| $p_e$ | $=p_b p_T \eta_h$ | 2.3.2 |

# Introduction

When two particles are connected so deeply that the state of one can not be described independently of the other, these particles are said to be entangled. Quantum entanglement is one of the most important aspects of quantum physics as it is inherently non-classical [1]. An entangled quantum system allows for many interesting applications like distributed quantum computing [2], superdense coding [3] and quantum cryptography [4], which would otherwise not be possible.
A widely used carrier of quantum information is the photon, the quantum of light. We can send and distribute these photons through optical fibers to create entanglement between distant nodes. However, optical fibres suffer from exponential losses [5], limiting achievable distances over which the photons can be distributed to a few hundred kilometers. As this is insufficient for global coverage, quantum repeaters have been proposed to extend the range of quantum networks [6]. Proof of principle quantum repeaters exist but are not quite practically useful yet. Despite the progress made on these quantum repeaters, a truly global quantum network based only on optical fibers and quantum repeaters still remains unfeasible. This is mainly caused by the high number of repeaters needed to make such a network usable in addition to limitations in where such a repeater can be placed. For example, due to high maintenance requirements it will be hard to place some quantum repeaters in the middle of the Atlantic ocean. These realisations led researchers to explore space-based segments, where losses scale more favourably with distance, because most of the transmission happens in free space rather then lossy fibres.
Satellite links are not just wishful thinking anymore, as the first quantum satellite named Micius was launched in 2016 [7], where quantum key distribution (QKD) was performed over a ground distance of 12000 km. For this satellite link, the transmission losses were at the order of 70 dB, compared to over 300 dB for a direct fibre link between the same ground stations.

In this work we compare three different satellite link schemes through analytical modelling. Connecting two ground stations via a direct downlink, a memory assisted downlink and a memory assisted uplink. Analytical models for static, symmetrical links for certain physical realizations have been made previously [8]. We extend this analysis by

1. making our model set up to be **applicable to a wide variety of physical realizations**, to be open to different hardware choices, as many options are still open and in development;

2. introducing **satellite movement**, which adds a complexity through time dependencies and asymmetrical links, and provides important insight into the way the rate of the protocol changes as the satellite flies over the ground stations. This also adds important parameters to be considered, like the height and inclination of the satellite orbit;

3. adding a **detailed transmission probability model**, including free space beam divergence, atmospheric effects, pointing losses and hardware losses depending on the positions of the ground stations and the satellite. This allows us to track the link losses at each point of the satellite's orbit and the position of the ground stations.

Our model can be used to define hardware requirements for certain setups, identify important parameters to focus improvement on, as well as explore the optimal scheme for existing and near-future available hardware.

We will first go over some background theory regarding quantum communication and satellite links in Chapter 1, which will help understand the derivation of our model in Chapter 2. The model is explained in 3 steps: we first outline a model for all components of the model in Section 2.1, we go over the way we keep track of positions of the ground stations and satellite in orbit, and our model for transmission probability in Section 2.2, we then put everything together to derive equations for the rate and fidelity for all schemes in Section 2.3. Lastly we look at some results of what we can learn from applying our model to different scenarios, which are reported and discussed in Chapter 3.

# Chapter 1

# Theory

Before we look at our model that we created to study the quantum satellite links, we first go over some concepts that will give appropriate background knowledge and help understand our model. We will first cover some basic concepts of quantum mechanics: entanglement and the no-cloning theorem. These concepts are at the heart of quantum communication and therefore important to our model. After covering the basic concepts we get more and more specific towards satellite based entanglement distribution: we will talk about quantum repeaters, loss and decoherence channels and go over the basics of satellite communication. Finally, we present a few possible applications of (satellite based) entanglement distribution.

## 1.1 Quantum entanglement

Two quantum systems are said to be entangled when we can not describe the state of one, without mentioning the other. This leads to correlated measurements of qualities of the quantum systems (violating the Bell inequality [9]), where, depending on the type of entanglement, the outcome of a measurement on the two systems is either always equal, or always opposite. A quantum system is *fully* entangled, when these correlations are perfect. Four well known examples of fully entangled quantum states are the so-called Bell states [10]:

$$|\phi^+\rangle = \frac{1}{\sqrt{2}}(|00\rangle + |11\rangle),$$
$$|\phi^-\rangle = \frac{1}{\sqrt{2}}(|00\rangle - |11\rangle),$$
$$|\psi^+\rangle = \frac{1}{\sqrt{2}}(|01\rangle + |10\rangle),$$
$$|\psi^-\rangle = \frac{1}{\sqrt{2}}(|01\rangle - |10\rangle).$$

Where $|0\rangle$ and $|1\rangle$ are the possible states of the quantum system, given in bra-ket notation, also known as Dirac notation [11]. For example, the states could be a spin up or down, the presence or absence of a photon, or horizontally or vertically polarized photons, depending on the system.
How much a system is entangled we can describe by what is called the fidelity of a state, often denoted by the letter $F$. A fully entangled state has fidelity 1, and the less correlations there are, the lower the fidelity. We can calculate the fidelity of a normalized quantum state $\rho$ with respect to a target state $|\phi^+\rangle$ as

$$F = \langle\phi^+|\rho|\phi^+\rangle. \tag{1.1}$$

The correlated measurements that are caused by the entanglement make for some interesting applications in the fields of quantum computing and quantum communication. In this thesis, we will focus our attention on applications in quantum communication, of which some are mentioned at the end of this Chapter (1.7).

## 1.2 No-cloning theorem

The no-cloning theorem states that it is not possible to create an identical copy of an arbitrary (unknown) quantum state. This allows for the security of the QKD protocol, but also hinders us in creating entanglement over long links.
To see how this works, consider a quantum state $|\Psi\rangle$ that we want to copy onto some initial or blank state $|e\rangle$. On our combined system $|\Psi\rangle \otimes |e\rangle$ we can perform either a measurement or unitary transformations. A measurement will lead to the collapse of the wavefunction, thereby destroying the information contained in $|\Psi\rangle$. Therefore our only option is to apply some unitary transformation $U$.
The no-cloning theorem then tells us that there is no unitary operator $U$, such that for all normalized states $|\Psi\rangle$ and $|e\rangle$ from Hilbert space $H$, we have

$$U|\Psi\rangle|e\rangle = e^{i\alpha}|\Psi\rangle|\Psi\rangle$$

for some real number $\alpha$.
To show this, we pick another state from the Hilbert space $|\Phi\rangle$, and use the fact that $U$ is unitary ($U^\dagger U = 1$) to find

$$\langle\Psi|\Phi\rangle\langle e|e\rangle = \langle\Phi|\langle e|U^\dagger U|e\rangle|\Psi\rangle = e^{i\alpha - i\beta}\langle\Phi|\langle\Phi||\Psi\rangle|\Psi\rangle = e^{i\alpha-i\beta}\langle\Phi||\Psi\rangle^2.$$

Since $|e\rangle$ is normalized ($|\langle e|e\rangle| = 1$), we then find that

$$|\langle\Psi|\Phi\rangle| = |\langle\Psi|\Phi\rangle|^2$$

For this to be true, we need that either $|\langle\Psi|\Phi\rangle| = 0$ (orthogonal states) or $|\langle\Psi|\Phi\rangle| = 1$ ($\Psi = e^{i\beta}\Phi$). While this is possible, this is not true for any arbitrary quantum state. Therefore $U$ cannot clone a *general* quantum state, thereby proving the no-cloning theorem.
So, we cannot just 'copy' a quantum state. What does this mean for us? On one hand, it means that also not any other person can copy a state that one might share with someone else, therefore making it impossible for a third party to listen in on a message one might send through the quantum link. On the other hand it also means that even the sender or anyone else can not copy the state, which makes it difficult to transport entangled particles, as in classical communication we can make use of repeaters, which receive an incoming message, copy it and redirect it, to extend transmissions so that the signal can cover longer distances. However, we just learned that this is not possible with quantum signals, which brings us to the topic of the next section, quantum repeaters.

## 1.3 Entanglement swapping and quantum repeaters

Due to the no-cloning theorem, we cannot simply copy-paste our photons, like in classical repeaters. But we still need a way to combat the high losses, which has lead to the idea of separating longer links into several smaller links, connected by quantum repeaters [12]. If we can create entanglement in two shorter links and use a protocol called entanglement swapping, we thereby extend the entanglement to a longer link.
To see how the protocol works, we consider 3 stations: Alice (A), Bob (B) and Carol (C). Carol shares an entangled pair with Alice, and one with Bob. This is visualized in Figure 1.1, where entanglement is indicated by a wavy line. Let's say they both share the Bell state $|\phi^+\rangle$, the combined state ABC is then given by

$$|\Psi\rangle_{A,B,C} = |\phi^+\rangle_{A,C_1}|\phi^+\rangle_{C_2,B}$$

Now Carol can perform a Bell state measurement (BSM), indicated as the big grey circle in Figure 1.1. This corresponds to measuring in a basis where the outcome is one of the 4 possible Bell states. When Carol measures the outcome to be $|\phi^+\rangle_{C1,C_2}$, our remaining state will be

$$\begin{aligned}
&\langle\phi^+|_{C_1,C_2}|\Psi\rangle_{A,B,C} \\
&= \langle\phi^+|_{C_1,C_2}\big(|00\rangle_{A,B}|00\rangle_{C_1,C_2} + |01\rangle_{A,B}|01\rangle_{C_1,C_2} + |10\rangle_{A,B}|10\rangle_{C_1,C_2} + |11\rangle_{A,B}|11\rangle_{C_1,C_2}\big) \\
&= |\phi^+\rangle_{A,B}.
\end{aligned}$$

Where we see that, as a result of the BSM by Carol, we end up with a Bell state shared between Alice and Bob! This means that we can now create longer entangled links by the use of a mid-point Carol.

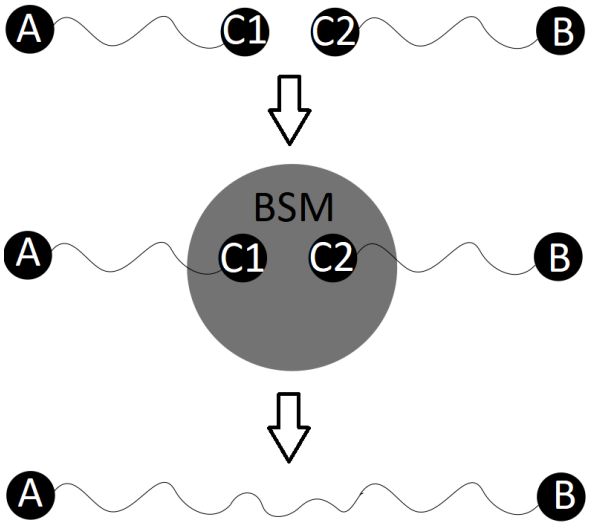


Figure 1.1: Visualization of the entanglement swapping protocol. Two entangled links (wavy lines) between Alice (A) and Carol (C1) and between Bob (B) and Carol (C2) are 'swapped' into a link between A and B by performing a Bell state Measurement (BSM, indicated by the big grey circle) on the qubits C1 and C2.

## 1.4 Photon loss and decoherence

In entanglement distribution, there are two main parameters that we are interested in. The first is the rate of the protocol, which is the amount of entangled pairs that are received per second. How many pairs we receive is determined by how many pairs we send, and how many we lose. Losing photon can be modelled by a *loss channel*.
When we have a probability $1-p$ of losing a photon, we can model this as applying a 'beam splitter' with transmittance $\sqrt{p}$ onto a loss mode $l_\sigma$. For some creation operator $c_\sigma^\dagger$. The loss channel is then given by

$$c_\sigma^\dagger \to \sqrt{1-p}l_{c,\sigma}^\dagger + \sqrt{p}c_\sigma^\dagger. \tag{1.2}$$

And since we do not really care about what happens to the photon after we lose it, we can trace out this loss mode.
The second important property of our entangled pairs is their fidelity: the quality of their entanglement. An entangled state can become less entangled over time, through a process called decoherence. Quantum decoherence transforms quantum probabilities into classical probabilities. Interactions with the environment can lead to the disappearance of the 'quantum behavior' of a system. This of often modelled with either a depolarizing channel or a dephasing channel. In our model, we will model all decoherence with depolarizing channels. Our state $\rho$ is mapped, with some probability $p$, onto the maximally mixed (classical) state $\frac{\mathbb{1}}{2} = \frac{1}{\sqrt{2}}(|0\rangle\langle 0| + |1\rangle\langle 1|)$:

$$\rho^{\text{depol}} = p\rho + (1-p)\frac{\mathbb{1}}{2}. \tag{1.3}$$

Now that we have gone over some concepts regarding quantum communication, we will turn our attention to satellite communication and configurations.

## 1.5 Zenith angle in satellite communication

To communicate with a satellite, it needs to be in our line of sight (i.e. not under the horizon). We can quantify this with a parameter called the zenith angle, denoted by $\zeta$. For any point on earth, you can find it's zenith by connecting a line from the centre of the earth through that point and out into

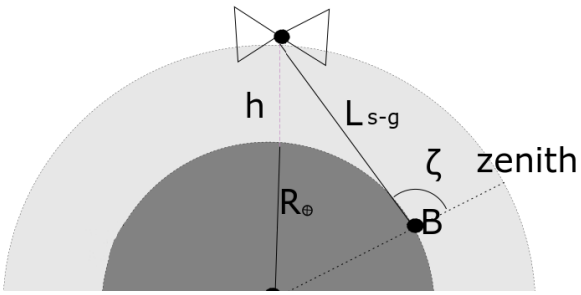


Figure 1.2: Representation of the terms 'zenith' and 'zenith angle'. We see ground station B on earth where a line from the centre of the earth through B signifies the term zenith. The angle between point B's zenith to the position of the satellite is the zenith angle, denoted by $\zeta$. h is the height of the satellite orbit, $L_{s-g}$ is the link length between B and the satellite and $R_{\oplus}$ is the radius of the earth.

the sky. The zenith angle of the satellite is then the angle from the satellite to that points zenith. An example of a configuration is shown in Figure 1.2, where the zenith angle of the satellite with respect to ground station B is indicated.
For the satellite to be above the horizon we only need $|\zeta| < 90°$, if we include mountains and tall buildings, this maximum angle becomes a bit lower. However, we also have to take into account that the bigger the zenith angle the longer the satellite link and the greater distance the signal has to travel through the atmosphere. For these reasons we generally restrict $|\zeta| < 70°$.

## 1.6 Satellite link configurations

There are many ways we can link two ground stations through a satellite, some of which are discussed in [13]. In this thesis we will go over three of these scenarios: a direct downlink, a memory assisted downlink and a memory assisted uplink. An overview of these configurations can be found in Figure 1.3. We study the direct downlink because it is the easiest and indeed the most direct way of creating entanglement between two points through a satellite link. By using the satellite as a quantum repeater we hope to make it feasible to create longer links in the memory assisted schemes. Throughout this thesis our model will outline advantages and disadvantages of each of these schemes such that we can make more informed decisions on which scheme is best suited for certain scenarios.

The direct downlink is the simplest case. We have our source, situated on the satellite, which sends down entangled photon pairs to the ground stations, which receive them and store them in a quantum memory.
In the memory assisted schemes, the satellite is used as a quantum repeater: entanglement is created in each arm separately, after which we perform the entanglement swapping protocol. For the memory assisted downlink, this means we need two sources and two memories on our satellite, as well as a way to perform the BSM. For the memory assisted uplink, the sources are located at the ground stations, along with a quantum memory. The satellite in the uplink also contains two quantum memories, and a BSM station.

## 1.7 Applications of entanglement in quantum communication

Now that we have discussed how we hope to make entanglement links, we will outline some common applications of entanglement in the field of quantum communication. We will not go into these too deep, as the main focus of the thesis will be on establishing entanglement between two distant parties, and not so much on what is done with this entanglement afterwards, but it is nevertheless interesting to consider some possibilities.

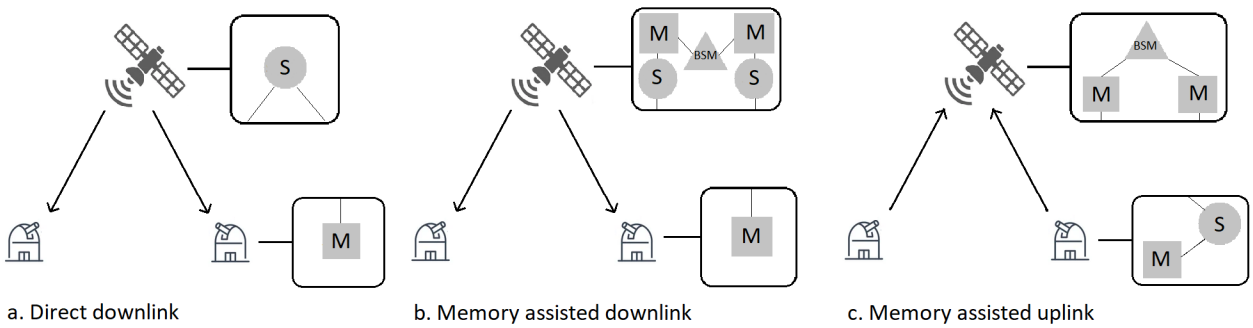


Figure 1.3: Different link configurations used in the model. a. Direct downlink: satellite containing an entangled photon source (circle), two receiving ground stations containing a quantum memory each (square). b. Memory assisted downlink: satellite containing two sources and two memories, as well as a BSM station (triangle) to perform the entanglement swap, two receiving ground stations with a quantum memory. c. Memory assisted uplink: two ground stations containing entangled photon sources and quantum memories and a receiving satellite with two quantum memories and a BSM station.

### 1.7.1 Quantum key distribution (QKD)

A message can be sent between two people as a (classical) string of bits. To make the message secret, so no people can listen in on your conversations, a key can be applied to the message, only known to the sender and receiver. When this key is generated by a QKD protocol, it is inherently secure, as the state can not be copied by anyone trying to listen in, due to the no-cloning theorem (described in Section 1.2). The third party trying to listen in could perform measurements, but not without letting their presence be know to the sender and receiver, as a measurement would destroy the entanglement. The most well-known QKD protocols are the BB84 protocol by Bennet and Brassard [14] and the E91 protocol by Artur Ekert [15].

### 1.7.2 Blind quantum computing

Delegated computation allows us to use central computers to run certain calculations that are not always suitable for personally owned hardware. It can be expected that with the development of quantum computers, there will also be a demand of delegated quantum computation. This is because quantum computers, especially in the beginning stages, will likely not be a common occurrence. With only a select few quantum computer available worldwide, it would be nice if these computers can be used by a wide variety of people from anywhere on earth.
While delegating calculations to remote systems may have strong practical and economic motivation, there are some security issues that come into play. The communication between the client and the quantum server can be protected via quantum cryptography such as QKD, which was described earlier. However, there lies a problem in the server itself being untrusted. Therefore, to have secure, correct results, we need the delegated tasks to be secure against the server executing them as well. This is known as blind quantum computing [16].
We could thus use our satellite links to make safe quantum computation possible for a wider audience.

### 1.7.3 Other applications

Some other interesting applications include:
Enhancing the precision of measurements, in a field called quantum metrology [17].
Sending more then one classical bit of information through one set of entangled pairs, this is known as superdense coding [3].
Quantum clock synchronization, which uses entanglement between two parties to establish a synchronized pair of atomic clocks [18].

# Chapter 2

# Model

In this chapter we will focus on the derivation of our model, which will consist of expressions for the rate and fidelity of schemes with a direct downlink, a memory assisted downlink or a memory assisted uplink. This is done by setting up models for what happens to a certain input state at each step in the schemes described in Section 2.1. Each subsection here can be seen as a puzzle piece, which are then put together to find the final expressions for rate and fidelity in Section 2.3. An important aspect of this model is how it tracks the links between the ground stations and the satellite and gives an expression for the transmission probability based on these links. An expression for this, as well as a description of how the satellite and ground station links are tracked, is derived in Section 2.2.

## 2.1 General models for protocol components

Here we will define our puzzle pieces. Each subsection describes a different part of the protocols. As the model contains a lot of different variables, we have compiled a list of all the variables, their meaning, and where they were introduced in the beginning of this thesis, which can be used for reference.

### 2.1.1 Entangled photon pair source

As a first step in distributing entangled photon pairs, we first need to create them. We look at a generic source for entangled photon pairs. As many different kinds of photon sources exist, we have made it possible to tweak the parameters introduced here to fit many different realizations of the source.
Spontaneous parametric down conversion [19] is a popular choice as entangled photon pair source. The downside of using this is the multi-photon events that can occur, limiting the fidelity. These events can be suppressed, but not without suppressing the overall rate. These properties of the SPDC lead to the choice of moving away from this source, using a general model for entangled pairs with no multi-photon events. This will lead to significant improvements in achievable rate and fidelity[1].
We assume that we create our target state, let's say $|\phi^+\rangle = \frac{1}{\sqrt{2}}(|1_\alpha 1_\alpha\rangle + |1_\beta 1_\beta\rangle)$, with some probability $p_0$, together with a random mixture of other states. We also have to take into account the generic source failing to emit a photon, with some probability $\sqrt{1-p_b}$. We can have a correlated loss probability for both photons, therefore we include a term $(1-p_b)|\varnothing\varnothing\rangle\langle\varnothing\varnothing|$ in our generated state.
A state generated by our generic source can be written as

$$\begin{aligned}\rho_{source} &= p_b(p_0|\phi^+\rangle\langle\phi^+| + p_{\alpha\alpha}|1_\alpha 1_\alpha\rangle\langle 1_\alpha 1_\alpha| + p_{\alpha\beta}|1_\alpha 1_\beta\rangle\langle 1_\alpha 1_\beta| \\ &\quad + p_{\beta\alpha}|1_\beta 1_\alpha\rangle\langle 1_\beta 1_\alpha| + p_{\beta\beta}|1_\beta 1_\beta\rangle\langle 1_\beta 1_\beta|) + (1-p_b)|\varnothing\varnothing\rangle\langle\varnothing\varnothing| \\ &= p_b\rho_\gamma + (1-p_b)|\varnothing\varnothing\rangle\langle\varnothing\varnothing|\end{aligned} \tag{2.1}$$

The source can also fail emit one photon with probability $1-p_w$, which is covered by applying a loss channel (discussed in Section 1.4). If the probability of getting zero photons is not the same as that of missing one, squared, this can be considered in the parameter $p_b$, otherwise it is taken care of in the

[1] The reason SPDC sources are still widely used is because other sources are not very well developed yet. However, this will not be the only time we are looking at future possibilities to try to make this optimistic goal of long entanglement links work.

loss channel.
This model does not take into account coherences (off-diagonal elements of the density matrix) since the two arms of the system will not interact, and therefore these elements will not affect the final fidelity.
As stated before, our model of a generic entangled photon pair source can fit many different sources. For example, in generation of polarization-entangled photons, using a quantum dot single photon source, linear optics and photodetectors [20], we will have $|1_\alpha\rangle = |\mathrm{H}\rangle$ and $|1_\beta\rangle = |\mathrm{V}\rangle$ and the components $p_{\alpha\alpha}$, $p_{\alpha\beta}$, $p_{\beta\alpha}$, $p_{\beta\beta}$ can be measured and are often represented in a 3D bar plot like in Figure 3 of [20]. Another possible encoding is time-bin encoding, like in [21]. These examples confirm the broad applicability of this component of our model.

### 2.1.2 Photon transmission

Now, we want to send our photons from the emitter to a receiver. In transmission we have a probability $1 - p_T$ of the photon getting lost. The photon transmission is modelled by a loss channel with probability $p_T$.
The transmission probability $p_T$ is derived in Section 2.2.3, where the zenith angle and link length can be kept track off using methods described in Section 2.2.1.
Transmission is only modelled through loss, since entanglement can survive after both entangled photons have passed through the atmosphere, as shown in [22][2]. If polarization encoding is used, one can compensate for the changing reference frame due to the motion of the satellite as described in [23][24].

### 2.1.3 Heralding

At several points in the protocols from Section 1.6, we make use of an heralding step, where we find out whether we have lost our photon, without having to measure it. Some memories herald the arrival and/or retrieval of a photon. Heralding can also be done using a quantum nondemolition detector (QND) [25].
When the probability of the photon being lost is high, we need to take into account dark counts, where the detector clicks even when our photon did not arrive. Depending on the type of memory or heralding that is used, dark counts can be modelled differently. In atomic ensemble memories, the read-out can reveal whether vacuum was stored in the memory due to a dark count. An example of this is given in [26] and [27], where a photon announces the mapping of a polarization state onto a magnon shared between two atomic ensembles. For these types of heralding, we will use the parameter $p_{\mathrm{dark,v}}$, which indicates that the dark count has been stored as a vacuum. Other memories where this way of modelling of dark counts would be suited are atomic frequency comb (AFC) type memories as in [28].
For some other types of memories, like ones based on spin systems [29], dark counts would be better modeled by introducing a probability of decoherence, as 'storing vacuum' would lead to reading out a certain state, instead of revealing that nothing was put in. This leads to the parameter $p_{\mathrm{dark,d}}$, where dark counts are stored as a completely decohered state.
The total effect of dark counts could thus be seen as some probability of decohering $p_{\mathrm{dark,\,d}}$ *or* some probability of storing your vacuum terms $p_{\mathrm{dark,\,v}}$, depending on your setup.
In the derivations following, we will neglect dark counts whenever the probability of a photon from the protocol being there to be heralded is relatively high, as the probability of having a dark count would be much lower than the probability of just heralding your photon as desired. If however the probability of the photon arriving at the heralding point is very low, like right after the transmission from satellite to ground or ground to satellite, we can not neglect this effect.
We should also take into account the heralding efficiency, where it does not herald the photon even though it was there. This photon is then essentially just lost, and we can take it into account by applying another loss channel with the heralding efficiency $\eta_h : \rho \to \eta_h\rho + (1 - \eta_h)|\varnothing\rangle\langle\varnothing|$.

[2]Some encodings actually do suffer from decoherence in the atmosphere, like using the orbital angular momentum of the photons, but those encodings are probably not the best choice for such protocols.

### 2.1.4 Quantum memory

To store a photon we need a quantum memory. There are many different types of quantum memories[3] and to try to include all of them into a single 'memory channel' we split all of the effects of the quantum memory on the state into two categories: loss and decoherence. This way, we can combine our loss and decoherence channels from Section 1.4. Loss and/or decoherence can occur in one of the three stages: loading the state into the memory, storing the state in the memory for some time $t$ and retrieving the state from the memory. But we will not know when exactly at which stage our loss or decoherence happens (and it also does not matter), so we can combine them into two terms: $\eta_{c,l}(t) = \eta'_{c,l}e^{-t/\tau}$ and $\eta_{c,d}(t) = \eta'_{c,d}e^{-t/\tau}$, indicating the probability of losing and decohering your quantum state, respectively. Here, $\tau$ signifies the memory coherence time and $\eta'_c$ is the zero-time memory efficiency in mode $c$.
We now define our memory channel as

$$\rho^{(c)} \to \eta_{c,l}(t_c)\eta_{c,d}(t_c)\rho + \eta_{c,l}(t_c)(1-\eta_{c,d}(t_c))\frac{\mathbb{1}}{2} + (1-\eta_{c,l}(t_c))|\varnothing\rangle\langle\varnothing|. \tag{2.2}$$

This equation shows that with a probability $\eta_{c,l}(t_c)\eta_{c,d}(t_c)$ our state has remained the same after storing it for a time $t_c$, with a probability $1-\eta_{c,l}(t_c)$ we lose our state and are left with a vacuum term and with a probability $\eta_{c,l}(t_c)(1-\eta_{c,d}(t_c))$ we still have our photon, but it has decohered.

### 2.1.5 Entanglement swap/BSM

In the memory assisted schemes, the satellite is used as a quantum repeater. Quantum repeaters were discussed in Section 1.3. For this protocol, entanglement is swapped by performing a Bell-state measurement (BSM) on one mode from each arm of the setup (Alice-satellite, Bob-satellite), thereby projecting the remaining photons at Alice and Bob's ground stations into an entangled state [30]. We can model the BSM by doing projective measurements in the Bell-basis with some efficiency $\eta^X$ ($X \in [\phi^{\pm}, \psi^{\pm}]$), and with some probability of depolarizing $1-p_{\text{BSM}}$, in case we detected the wrong Bell state[4]. This will look like

$$\begin{aligned}\rho \to & p_{\text{BSM}}\Big(\eta^{\phi^+}\langle\phi^+|\rho|\phi^+\rangle + \eta^{\phi^-}Z\langle\phi^-|\rho|\phi^-\rangle Z^\dagger + \eta^{\psi^+}X\langle\psi^+|\rho|\psi^+\rangle X^\dagger \\ & + \eta^{\psi^-}XZ\langle\psi^-|\rho|\psi^-\rangle(XZ)^\dagger\Big) + (1-p_{\text{BSM}})\frac{\mathbb{1}}{2}\otimes\frac{\mathbb{1}}{2}.\end{aligned} \tag{2.3}$$

Where $\eta^{\psi^+} + \eta^{\psi^-} + \eta^{\phi^+} + \eta^{\phi^-} = 1$ and are determined by the probability of detecting each state. An example of these parameters is given in Figure 4 of [31].
Since the outcome of the BSM will reveal if there were photons being measured or not, we can trace out any vacuum terms and normalize the state after this step.
Dark counts are not included as we will be in the regime where $1-\langle\varnothing|\rho|\varnothing\rangle \ll p_{\text{dark}}$ because the BSM is performed on the modes that were directly taken out of the memory and we don't expect very high losses here.
For the rate of the protocol, we will also include an extra parameter $\eta_{\text{BSM}}$. This parameter takes into account that we can not always distinguish all our states, like in linear optics, where $\eta_{\text{BSM}} = 1/2$ as only the odd parity sates $|\psi^{\pm}\rangle$ can be successfully detected and distinguished [32], which will half the rate.
Since fidelity is an often reported number, we can use this to find $p_{\text{BSM}}$ in our model: $p_{\text{BSM}} + (1-p_{\text{BSM}})/4 = \text{F}_{\text{BSM}}$. We assume that the single qubit rotation gates are perfect, since they will probably not be done in practice as for most applications it does not matter which of the Bell states comes out. However, we have them in the model as it makes it easier for the calculations to get a final average fidelity.

[3] Note that this has to be a memory with on-demand retrieval, which limits choice in possible physical realizations.
[4] If we measure that we are in state x, but we were actually in state y, this would lead to terms to which we apply the wrong rotations, which we bunch into one term as complete depolarizing. This is a worst-case scenario way of modelling this effect.

## 2.2 Orbits

This Section will focus on the links between the ground stations and the satellite. We first describe a way to track positions, then we go into a derivation that uses these positions to find the transmission probability for each ground station at each point of the satellites orbit.

### 2.2.1 Satellite path and zenith angles

Here, we find a way to express the position of the ground stations and satellite at each point in time, taking into account the rotation of the earth and the orbit of the satellite. With this we can track the length of the link, as well as the zenith angle of the link.
A simple way to keep track of all of these positions is in terms of vectors, that way, we can easily calculate distances and angles. It is easy to find the coordinates of any place in terms of x degrees (°) north or south and y degrees east or west on a map. If we define north and east as our 'positive' directions, then we can convert this into polar coordinates to find the position of our ground station (gs) at a time $t$ as

$$\mathbf{x}_{\text{gs}}(t) = \begin{bmatrix} R_\oplus \sin(90° - x°)\cos(y° + \theta_e t) \\ R_\oplus \sin(90° - x°)\sin(y° + \theta_e t) \\ R_\oplus \cos(90° - x°) \end{bmatrix}. \tag{2.4}$$

Where $R_\oplus$ is the radius of the earth, and $\theta_e$ is the angular velocity of the earth's rotation ($2\pi$ radians per 24 hours).
To be able to keep track of the position of the satellite, we first need to know what its orbit will look like. If we assume that the orbit is circular, the path is determined by two parameters: the height of the orbit $R_\oplus + h$ and the inclination $\alpha$. The inclination angle of an orbit is how far the orbit is tilted with respect to the equatorial plane, visualized in Figure 2.1. The position of the satellite at any point in time $t$ can then be found as

$$\mathbf{x}_{\text{sat}}(t) = R_x(\alpha) \begin{bmatrix} (R_\oplus + h)\cos(\theta_s t) \\ (R_\oplus + h)\sin(\theta_s t) \\ 0 \end{bmatrix}. \tag{2.5}$$

With $R_x(\alpha)$ the rotation matrix for an angle $\alpha$ around the x-axis and $\theta_s$ the angular velocity of the satellite. The angular velocity is given by $2\pi/T$ where $T = 2\pi\sqrt{(R_\oplus + h)^3/GM_\oplus}$ is the orbital period of the satellite, $G$ is the gravitational constant and $M_\oplus$ is the mass of the earth.
In reality an orbit is never perfectly circular, and sometimes not circular at all, for eccentricities $\neq 0$ we could keep track of the orbit similar to what is done in [33]. However, the equations used there are a lot more complicated and for near-circular orbits this will not lead to significant changes in our final rate or fidelity.
We can choose the height and inclination angle of the satellite with some limitation related to the satellite design. For example, for certain combinations of satellite heights with inclination angles, the orbit can be sun-synchronous, which among other things has a positive impact on the thermal design of the satellite [34] as well as giving the advantage of the satellite flying over at the same time every day. The first quantum satellite, Micius, is also in sun-synchronous orbit [7].
With the coordinates of the ground stations and satellite we can find the zenith angle for each ground station at each point in time using the dot product rule:

$$\zeta = \arccos\left(\frac{\mathbf{a}\cdot\mathbf{b}}{|\mathbf{a}||\mathbf{b}|}\right). \tag{2.6}$$

Here, $\mathbf{a}$ is a vector connecting the ground station to the satellite (given by $\mathbf{x}_{\text{sat}} - \mathbf{x}_{\text{gs}}$) and $\mathbf{b}$ is the location of the ground station ($\mathbf{x}_{\text{gs}}$). And the link length is given by $L = |\mathbf{a}|$.

Now we know, for each point in time, what the zenith angle and link length of the satellite with respect to our ground stations are.

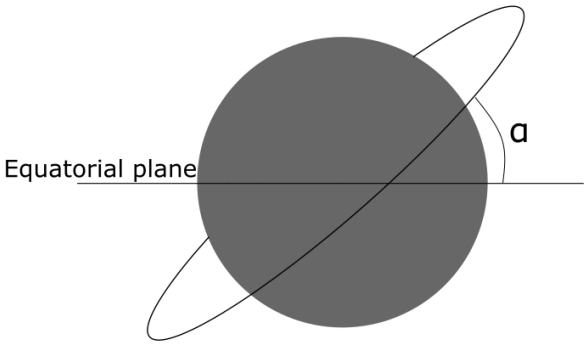


Figure 2.1: The inclination angle $\alpha$ of an orbit is the tilt with respect to the equatorial plane.

### 2.2.2 Communication window

The communication window is a window in time where the satellite is at a position where it can communicate with both ground stations. The communication window is defined by having the zenith angle of both ground stations below 70°[5]. This can be relaxed a bit for the memory assisted schemes, because the ground stations do not need to receive the photons from the same created pair and there can thus be entanglement generated in one arm before the satellite can communicate with the other ground station.
If we call the area where the satellite is within $\zeta < 70°$ window 1 for one ground station, and window 2 for the other ground station, then our total communication window for the direct downlink case is where the satellite is in window 1 at a time t and also in window 2 at that same time. For the memory assisted schemes, this extends to being in window1 at a time t and in window 2 at t + some cutoff time later. This cutoff time is determined by the coherence time of the memory. Currently memory coherence times are too short for this window increasing effect to be significant, but it is an advantage when coherence times become in the order of minutes.

### 2.2.3 Transmission probability

Now that we can track the links, we will derive expressions for the probability that a photon reaches the receiver once it has been emitted successfully.
The beam effects of Equations 2.7-2.10 are based on Section 8.1.9 of [35], focusing on long term beam effects.
We start off by assuming we are dealing with a Gaussian beam, with beam waist (=most narrow part of the beam) $w_0$ and intensity $I_0$. For the free space propagation we have the effect of divergence, meaning that the width of the beam increases. The beam width affects how many photons reach the receiver due to the finite size of the receiver aperture. The beam size as a function of propagation distance $z$, not including atmospheric effects, is given by

$$w(z)^2 = w_0^2 \left[1 + \left(\frac{z}{Z_0}\right)^2\right]. \tag{2.7}$$

Here, $Z_0 = \frac{\pi w_0^2}{\lambda}$ is the Rayleigh distance. The beam waist can also be calculated using the divergence angle $\theta$ as $w_0 = \frac{\lambda}{\pi\theta}$ [36][6].
Turbulence in the atmosphere will induce further spreading of the beam, leading to an effective beam width of

$$w_{eff}(z)^2 = w(z)^2(1 + T). \tag{2.8}$$

[5]See Section notes on orbits at the end of Section 2.2.3.

[6]Usually the beam waist is known as this corresponds to the emitter radius, and the divergence angle can be calculated from this, but sometimes only the divergence angle is reported so it may be useful to have this expression for those occasions.

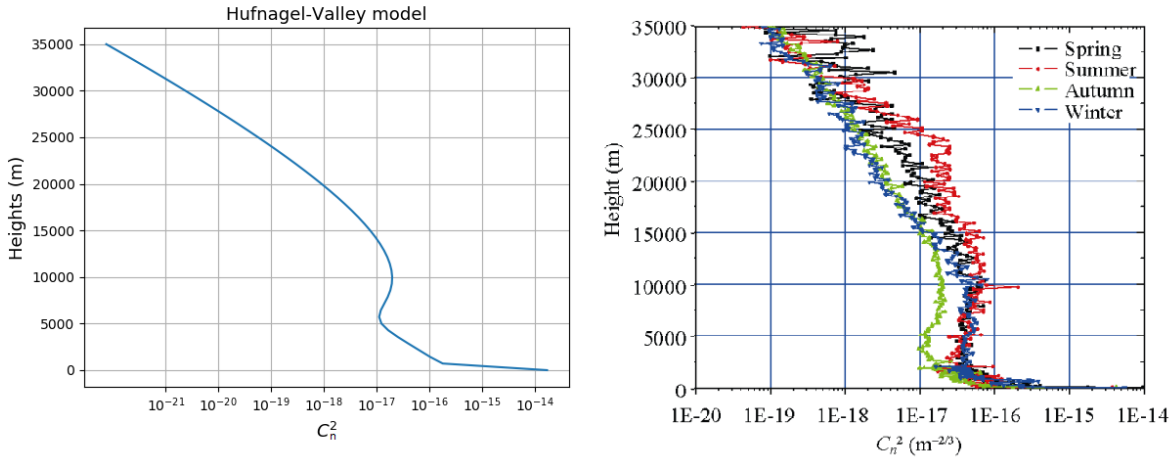


Figure 2.2: Comparison of the Hufnagel-Valley model of the index structure constant as a function of the height above the earths surface (left) calculated with 50 data points, compared to measurements by [39] (right). For a height above 20000 meters the model slightly underestimates the index structure constant. We see that the Hufnagel-Valley approximates the behavior found in measurements reasonably well.

This T, describing the additional spreading of the beam due to turbulence, is for an uplink given by

$$T_{\text{up}} = 4.35\Lambda^{5/6}k^{7/6}L^{5/6}\sec^{11/6}(\zeta)\int_{h_0}^{h_0+L} C_n^2(h)\left(1-\frac{h-h_0}{L}\right)^{5/3}\mathrm{d}h, \tag{2.9}$$

and for a downlink

$$T_{\text{down}} = 4.35\Lambda^{5/6}k^{7/6}L^{5/6}\sec^{11/6}(\zeta)\int_{h_0}^{h_0+L} C_n^2(h)\left(\frac{h-h_0}{L}\right)^{5/3}\mathrm{d}h, \tag{2.10}$$

for a ground station at altitude $h_0$ and a satellite at altitude $h_0 + L$. Where, $\Lambda = \frac{2z}{kw(z)^2}$, $k$ is the wavenumber, $\zeta$ is the zenith angle, and $C_n^2$ is the index structure constant, which we can model with the Hufnagel-Valley model [37]:

$$\begin{aligned} C_n^2 =& 0.00594(v/27)^2(10^{-5}h)^{10}\exp(-h/1000) \\ &+ 2.7\cdot 10^{-16}\exp(-h/1500) \\ &+ A\exp(-h/100), \end{aligned} \tag{2.11}$$

with $v = 21$ m/s as the default wind speed at high altitude[7] and $A = 1.6\cdot 10^{-14}\text{m}^{-2/3}$ the turbulence strength at the ground level.
The Hufnagel-Valley model is an empirical model of the index structure constant. To test how it performs, we compared it to the measurements by [39] in Hefei, which can be seen in Figure 2.2. As expected we see that the model correctly reproduces the measured data, except it slightly underestimates $C_n^2$ for the highest altitudes, but as it is such a low number, this will not lead to a significant difference in transmission probability.

Now we have included beam divergence due to free space propagation and due to atmospheric effects. We can use this beam size to calculate the fraction of the beam that is picked up by the receiver.
For a Gaussian beam, the intensity is given by

$$I(r,z) = I_0\left(\frac{w_o}{w(z)}\right)^2\exp\left(\frac{-2r^2}{w(z)^2}\right). \tag{2.12}$$

[7]The wind speed can more accurately be described by the Bufton model like in [38], but it won't make a significant difference in these calculations.

Here, $I_0 = \frac{2P_0}{\pi w_0^2}$, with $P_0$ the power at the beam center, is the intensity at the center of the beam waist and r is the radial distance from the centre of the beam. From this, we can calculate the power $P_R$, that ends up at the receiver by integrating over the (circular) receiver aperture with radius R:

$$P_R = 2\pi I_0 \int_0^R \rho \exp\left[-2\left(\frac{\rho^2}{w(L)^2}\right)\right] \mathrm{d}\rho. \tag{2.13}$$

Finally, we have our total transmission probability given by

$$\begin{aligned} p_T &= L_p L_T L_R L_{ATM} L_j (P_R/P_E) \\ &= \eta_0 \left(1 - e^{-2R^2/w_{\text{eff}}(L)^2}\right). \end{aligned} \tag{2.14}$$

Where $L_p$ are the pointing losses, $L_T$ and $L_R$ are the transmitter and receiver (hardware) losses, like the effects of obscured apertures discussed in [40], $L_j$ is jitter loss (dynamic pointing loss) and $L_{ATM} = 10^{-\frac{4.34\tau(0)\sec(\zeta)}{10}}$ [35] is loss due to regular extinction, by scattering and absorption in the atmosphere. $\tau(0)$ is the path depth at the zenith (determined by the atmospheric transmittance for the wavelength used).
With this we can calculate the transmission probability for any configuration of ground stations and satellite at any point in time.

**Some notes on transmission probability and orbits**

The model assumes a flat earth. With large ground distances we might need some geometric correction. If we keep our zenith angle below 70°, this error should be quite small. We can leave out the bigger zenith angles as there the photon would travel a much larger distance through the atmosphere, leading to greater losses. However, sometimes the rate might be so low that a small extension of the communication window may be favourable. Since the biggest factor in the transmission probability is the broadening of the beam depending on the link length, which is still calculated correctly by the model, it will still give a good approximation.
Jitter and pointing losses are less significant if the beam is broader, therefore one could choose to somewhat increase the beam waist when these losses are significant, to find a balance between the two.
Determining the height of the satellite comes with a trade-off. A higher satellite orbit will lead to longer link lengths and thus higher transmission loss, which lowers the rate of the protocol. A lower orbit, however, will lower the time available to communicate with the satellite in the two following ways. In order to perform the protocol, the satellite needs to be in the communication window, meaning $\zeta < 70°$, for both ground stations. This window is a smaller 'area' for a low orbit than for a higher orbit. In addition to this, the orbital velocity of the satellite goes up the closer it gets to earth, which decreases your time to communicate with it even further.
The increased loss in transmission for longer links is why most work has been focused on low earth orbit (LEO) satellites. To bridge larger distances, like intercontinental links, we must either go to a medium earth orbit (MEO) or have multiple satellites and create inter-satellite links, because the satellite will otherwise never be in the communication window. Since this work focuses on single satellite links, this means we will be looking at MEOs. The height must be large enough such that the communication window is at least larger than the average time it takes for one (or more if desired) entangled pair to be distributed.
In this thesis we do not focus on optimizing the orbit of the satellite. More information on how different orbits affect the rate and communication time can be found in [41].

## 2.3 Rate and fidelity derivations

In this Section we will use the model components of the previous section and apply them to the scenarios direct downlink, memory assisted downlink and memory assisted uplink, as discussed in Section 1.6, to derive equations for the fidelity and rates of the schemes.

### 2.3.1 Direct downlink

The direct downlink scenario consists of two ground stations equipped with a photon receiver and quantum memory with $N_{\text{mem}}$ memory slots available and a satellite containing the entangled photon

source. With a repetition rate of $r_{\text{rep}}$ we send down one photon of an entangled pair to each ground station. When the photon is received on the ground, it is put into one of the memory slots, where it is stored until a (classical) signal from the other ground station arrives confirming that it also received their half of the entangled pair. When no signal is received within the communication time between the two ground station the attempt has failed and the memory resets. The communication time is given by $T_{\text{gcom}} = L_g/v_\gamma$, with $L_g$ the distance between the ground stations and $v_\gamma$ the speed of light in the fibre ($v_\gamma = c/\text{refractive index}$, refractive index of fiber $\approx 1.4$).
The average duration before a photon reaches the ground station such that the photon can be stored is about $1/p_T r_{\text{rep}}$ seconds, with $p_T$ the transmission probability. In most cases, we will be in the regime where $N_{\text{mem}}/p_T r_{\text{rep}} \gg T_{\text{gcom}}$, such that we know when the protocol failed and we can reset the memory quicker than we can fill up the memory. Therefore, we can keep sending down photons from the satellite instead of waiting to see if the protocol succeeded before each new try.
For this scheme, we thus undergo the following steps:

1. Entangled photon pairs are created (eq. 2.1 + loss channel with a probability of failing to emit a photon of $1 - p_w$) with repetition rate $r_{\text{rep}}$;
2. the photons are transmitted to the ground stations, modeled by a loss channel with probability $p_T$ of successful transmission (eq. 1.2). This loss is different in each arm and time dependent due to the orbits of the satellite and earth (as described in Section 2.2);
3. the arrival of the photons is heralded with efficiency $\eta_{h,1}$ and dark count probability $p_{\text{dark,v}}$ or $p_{\text{dark,d}}$, Alice and Bob share their results through a classical communication channel (this takes $T_{\text{gcom}}$);
4. the photons are loaded into the memory and stored until the stations know that each of them received the photon, or the memory is reset when no signal arrives;
5. heralded retrieval from the memory ($\eta_{h,2}$). This step is optional.

We find the rate of the protocol as the probability of both photons from the entangled pair retrieved and heralded from the memory correctly, multiplied by the repetition rate of the source[8].

$$\boxed{R = p_b p_w^2 p_{T,a}(t) p_{T,b}(t) \eta_{h,1}^2 p_{a,a} p_{a,b} \eta_{a,l}(t) \eta_{b,l}(t) \eta_{h,2}^2 r_{rep}} \tag{2.15}$$

Here, $p_b p_w^2$ indicates that two photon pairs were created successfully by the source, $p_{T,c}$ is the transmission probability for the photon from mode $c$, $\eta_h$ is the heralding efficiency, $p_a$ represents the probability that there is space in the memory for a photon to be stored, and $\eta_{c,l}(t)$ is the loss-efficiency of the memory after loading the state from mode $c$ into the memory and then storing it for a time $t$.
If step 5, the second heralding step, is not used, we can simply leave out the $\eta_{h,2}$ of Equation 2.15. This might be the case when your memory retrieval is not automatically heralded and you do not want to add an extra step to the protocol to take care of the heralding.
We can find $p_a$ as [8]

$$p_a = \sum_{k=0}^{N_{\text{mem}}} P_{\text{Binom}}(k, T_{\text{gcom}} r_{\text{rep}}, p_a p_e), \tag{2.16}$$

where $p_e = p_b p_w^2 p_T \eta_{h,1}$ and $P_{\text{Binom}}$ is the binomial distribution given by

$$P_{\text{Binom}}(k, n, p) = \binom{n}{k} p^k (1-p)^{n-k}. \tag{2.17}$$

Since $p_e \ll 1$ and $T_{\text{gcom}} r_{\text{rep}} \gg 1$, we can approximate this expression as

$$p_a = \sum_{k=0}^{N_{\text{mem}}} P_{\text{Pois}}(k, p_a T_{\text{gcom}} r_{\text{rep}} p_e), \tag{2.18}$$

with $P_{\text{Pois}}(k, \lambda)$ the Poisson distribution. This makes $p_a$ easier to find, especially when the number of memory slots $N_{\text{mem}}$ is large.

[8] This expression neglects dark counts. For the full expression including dark counts see Equation A.1 in the Appendix

**Fidelity**

To calculate the fidelity, we start off with Equation 2.1, for the source, and apply three loss channels to both modes. One loss channel will be for the source, which fails to emit a photon with probability $1-p_w$. The next loss channel is for the transmission from satellite to ground, where the transmission is successful with probability $p_{T,c}$ ($c \in [a,b]$). The last loss channel takes into account heralding efficiency, $\eta_{h,1}$. We discard all the terms where we do not herald both photons. Taking into account dark counts, we may falsely herald some states, keeping the vacuum terms with probability $p_{\text{dark,v}}$ or storing a maximally mixed, depolarized state with probability $p_{\text{dark,d}}$.
Our state after creation, transmission and heralding of the photon is then given by

$$\begin{aligned}\rho_{\text{herald}}^{(a,b)} =& A\rho_\gamma + B|\varnothing\rangle\langle\varnothing| \otimes \text{Tr}_a(\rho_\gamma) + C\text{Tr}_b(\rho_\gamma) \otimes |\varnothing\rangle\langle\varnothing| + D\text{Tr}_b(\rho_\gamma) \otimes \frac{\mathbb{1}}{2} \\ &+ E\frac{\mathbb{1}}{2} \otimes \text{Tr}_a(\rho_\gamma) + F\frac{\mathbb{1}}{2} \otimes \frac{\mathbb{1}}{2} + G|\varnothing\varnothing\rangle\langle\varnothing\varnothing| + H\frac{\mathbb{1}}{2} \otimes |\varnothing\rangle\langle\varnothing| + I|\varnothing\rangle\langle\varnothing| \otimes \frac{\mathbb{1}}{2},\end{aligned} \tag{2.19}$$

where

$$\begin{aligned}A =& p_{\text{suc}} = p_b p_{h,a} p_{h,b}; \\ B =& p_{\text{lose a}} p_{\text{dark,v}} = p_b(1-p_{h,a}) p_{h,b} p_{\text{dark,v}}; \\ C =& p_{\text{lose b}} p_{\text{dark,v}} = p_b p_{h,a}(1-p_{h,b}) p_{\text{dark,v}}; \\ D =& p_{\text{lose b}} p_{\text{dark,d}}; \\ E =& p_{\text{lose a}} p_{\text{dark,d}}; \\ F =& p_{\text{lose both}} p_{\text{dark,d}}^2 = \big((1-p_b) + p_b(1-p_{h,a})(1-p_{h,b})\big) p_{\text{dark,d}}^2; \\ G =& p_{\text{lose both}} p_{\text{dark,v}}^2; \\ H =& p_{\text{lose both}} p_{\text{dark,v}} p_{\text{dark,d}}; \\ I =& p_{\text{lose both}} p_{\text{dark,v}} p_{\text{dark,d}}.\end{aligned} \tag{2.20}$$

Here, $p_{\text{suc}}$ is the probability that both photons reach the ground stations successfully, and thus no photon is lost in any of the loss channels. $p_{\text{lose a,b}}$ represents the probability that Alice's or Bob's photon is lost in any of the loss channels and $p_{\text{lose both}}$ is the probability that both photons are lost somewhere in those three steps. These probabilities are given in terms of the probability of heralding a photon, which includes the probability of (not) failing to emit a photon from the source, transmission probability and heralding efficiency, with the time dependency omitted: $p_{h,c} = p_w p_{T,c}(t) \eta_{h,1}$. The terms H and I will be zero as we will either model dark counts as decoherence or vacuum, so either $p_{\text{dark,d}} = 0$ or $p_{\text{dark,v}} = 0$.
We can normalize our heralded state as

$$\rho_{\text{h}}^{(a,b)} = \rho_{\text{herald}}^{(a,b)} / \text{Tr}(\rho_{\text{herald}}^{(a,b)}) \tag{2.21}$$

Next, we will load this state into a memory to store until use. We model this by applying our 'memory channel' from Equation 2.2 to both modes to get to the state of the qubits stored in Alices and Bobs memories as

$$\begin{aligned}\rho_{\text{h}}^{(a,b)} \xrightarrow{\text{memory}} \rho_{\text{mem}}^{(a,b)} =& A'\rho_\gamma + B'|\varnothing\rangle\langle\varnothing| \otimes \text{Tr}_a(\rho_\gamma) + C'\text{Tr}_b(\rho_\gamma) \otimes |\varnothing\rangle\langle\varnothing| + D'\text{Tr}_b(\rho_\gamma) \otimes \frac{\mathbb{1}}{2} \\ &+ E'\frac{\mathbb{1}}{2} \otimes \text{Tr}_a(\rho_\gamma) + F'\frac{\mathbb{1}}{2} \otimes \frac{\mathbb{1}}{2} + G'|\varnothing\varnothing\rangle\langle\varnothing\varnothing| + H'\frac{\mathbb{1}}{2} \otimes |\varnothing\rangle\langle\varnothing| + I'|\varnothing\rangle\langle\varnothing| \otimes \frac{\mathbb{1}}{2},\end{aligned} \tag{2.22}$$

Where

$$
\begin{aligned}
A' =& p_{\text{suc}}\eta_{a,l}\eta_{b,l}\eta_{a,d}\eta_{b,d}/\text{Tr}(\rho^{(a,b)}_{\text{herald}}),\\
B' =& \left(p_{\text{lose a}}p_{\text{dark,v}}\eta_{b,l}\eta_{b,d} + p_{\text{suc}}(1-\eta_{a,l})\eta_{b,l}\eta_{b,d}\right)/\text{Tr}(\rho^{(a,b)}_{\text{herald}}),\\
C' =& \left(p_{\text{lose b}}p_{\text{dark,v}}\eta_{a,l}\eta_{a,d} + p_{\text{suc}}\eta_{a,l}(1-\eta_{b,l})\eta_{a,d}\right)/\text{Tr}(\rho^{(a,b)}_{\text{herald}}),\\
D' =& \left(p_{\text{lose b}}p_{\text{dark,d}} + p_{\text{suc}}\eta_{a,l}\eta_{b,l}\eta_{a,d}(1-\eta_{b,d})\right)/\text{Tr}(\rho^{(a,b)}_{\text{herald}}),\\
E' =& \left(p_{\text{lose a}}p_{\text{dark,d}} + p_{\text{suc}}\eta_{a,l}\eta_{b,l}(1-\eta_{a,d})\eta_{b,d}\right)/\text{Tr}(\rho^{(a,b)}_{\text{herald}}),\\
F' =& \left(p_{\text{lose both}}p^2_{\text{dark,d}} + p_{\text{suc}}\eta_{a,l}\eta_{b,l}(1-\eta_{a,d})(1-\eta_{b,d})\right)/\text{Tr}(\rho^{(a,b)}_{\text{herald}}),\\
G' =& \left(p_{\text{lose both}}p^2_{\text{dark,v}} + p_{\text{lose a}}p_{\text{dark,v}}(1-\eta_{b,l}) + p_{\text{lose b}}p_{\text{dark,v}}(1-\eta_{a,l}) + p_{\text{suc}}(1-\eta_{a,l})(1-\eta_{b,l})\right)/\text{Tr}(\rho^{(a,b)}_{\text{herald}}),\\
H' =& \big(p_{\text{lose both}}p_{\text{dark,v}}p_{\text{dark,d}} + p_{\text{lose b}}p_{\text{dark,v}}\eta_{a,l}(1-\eta_{a,d}) + p_{\text{lose a}}p_{\text{dark,d}}\eta_{a,l}(1-\eta_{b,l})\\
&+ p_{\text{suc}}\eta_{a,l}(1-\eta_{b,l})(1-\eta_{a,d})\big)/\text{Tr}(\rho^{(a,b)}_{\text{herald}}),\\
I' =& \big(p_{\text{lose both}}p_{\text{dark,v}}p_{\text{dark,d}} + p_{\text{lose a}}p_{\text{dark,v}}\eta_{b,l}(1-\eta_{b,d}) + p_{\text{lose b}}p_{\text{dark,d}}\eta_{a,l}(1-\eta_{b,l})\\
&+ p_{\text{suc}}(1-\eta_{a,l})\eta_{b,l}(1-\eta_{b,d})\big)/\text{Tr}(\rho^{(a,b)}_{\text{herald}}).
\end{aligned}
\tag{2.23}
$$

In many cases the retrieval from the memory will also be heralded, therefore we include another heralding step before Alice and Bob start to use their photons for their chosen protocol. We take the terms from Equation 2.22 and act on it with a loss channel to model the non-unit heralding efficiency $\eta_{h,2}$. Since entering into the memory was already heralded, the probability of getting a vacuum term out of the memory will be small enough to neglect dark counts. We then find

$$
\rho^{(a,b)}_{\text{mem}} \xrightarrow{\text{heralding}} \rho^{(a,b)}_{\text{mem, herlad}} = A''\rho_\gamma + D''\text{Tr}_b(\rho_\gamma)\otimes\frac{\mathbb{1}}{2} + E''\frac{\mathbb{1}}{2}\otimes\text{Tr}_a(\rho_\gamma) + F''\frac{\mathbb{1}}{2}\otimes\frac{\mathbb{1}}{2}, \tag{2.24}
$$

with

$$
\begin{aligned}
A'' =& \eta^2_{h,2}A',\\
D'' =& \eta^2_{h,2}D',\\
E'' =& \eta^2_{h,2}E',\\
F'' =& \eta^2_{h,2}F'.
\end{aligned}
\tag{2.25}
$$

This can again be normalized to find our final state

$$
\rho^{(a,b)}_{\text{final}} = \rho^{(a,b)}_{\text{mem, herald}}/\text{Tr}(\rho^{(a,b)}_{\text{mem, herald}}). \tag{2.26}
$$

Finally, our fidelity with respect to $|\phi^+\rangle$ is given by

$$
\begin{aligned}
F(t) =& \langle\phi^+|\rho_{\text{final}}|\phi^+\rangle\\
=& \boxed{(p_0 + \frac{p_{\alpha\alpha}}{2} + \frac{p_{\beta\beta}}{2})\frac{A''}{\text{Tr}(\rho^{(a,b)}_{\text{mem, herald}})} + \frac{1}{4}(p_0 + p_{\alpha\alpha} + p_{\alpha\beta} + p_{\beta\beta} + p_{\beta\alpha})\frac{(D''+E'')}{\text{Tr}(\rho^{(a,b)}_{\text{mem, herald}})} + \frac{F''}{4\text{Tr}(\rho^{(a,b)}_{\text{mem, herald}})}.}
\end{aligned}
\tag{2.27}
$$

This depends both on the time of emission and the time the qubits have been stored in the memories. If the protocol does not require or does not have an heralding step, Equation 2.27 can be used with a little modification: remove the heralding step by erasing the trace terms (set $\text{Tr}(\rho^{(a,b)}_{\text{mem, herald}})$ to 1) and use A', D', E' and F' from Equation 2.23 instead of the double-primed versions from Equation 2.25:

$$
\begin{aligned}
F_{\text{not heralded}}(t) =& \langle\phi^+|\rho_{\text{final, not heralded}}|\phi^+\rangle\\
=& \boxed{(p_0 + \frac{p_{\alpha\alpha}}{2} + p_{\beta\beta}2)A' + \frac{1}{4}(p_0 + p_{\alpha\alpha} + p_{\alpha\beta} + p_{\beta\beta} + p_{\beta\alpha})(D'+E') + \frac{F'}{4}}
\end{aligned}
\tag{2.28}
$$

This model is compared to data from the Micius satellite as reported in [42]. The results show good agreement and can be found in Section 2.4.

### 2.3.2 Memory assisted downlink

The downside of the direct downlink scheme discussed in the previous section is the need for both photons of one pair to arrive at the ground stations. This means that the success probability scales with the transmission probability squared. With the low transmission probability being the main issue in scaling to larger distances, this is a problem. If we, however, introduce assisting memories on the satellite, we can create entanglement in each arm independently, such that it scales linearly with $p_T$. The scheme uses two photon sources and 4 memories. Two memories are located on the satellite and ideally have a good multimode capacity, such that we can store $N_{\text{mem}}$ photons. The other two memories are kept at the receivers on the ground, which serve the same purpose as in the direct downlink scheme.
With a repetition rate of $r_{\text{rep}}$, $N_{\text{mem}}$ entangled photon pairs are created in each arm of the setup. One photon of each pair is stored in the memory on the satellite with memory efficiency $\mu$ and the other is sent down to the receiver on the ground, where it will also be stored in a memory with efficiency $\eta$ until the heralding signal arrives back at the satellite for both arms and the entanglement swap is performed.
We will look at the rate of this scheme, defined as the average number of entangled photon pairs received per second. After that we use this to find the average fidelity of those arrived pairs, using again the protocol components from Section 2.1.

#### Rate

We will now turn to setting up an expression to capture the average number of entangled photon pairs received. In this calculation, time windows will be important, an overview of these times can be found in Figure 2.3. The protocol starts off by creating $N_{\text{mem}}$ photon pairs per arm, and sending half of each pair down. The time it takes to generate these $N_{\text{mem}}$ photon pairs and 'fire' half of each pair down, we will call $t_{\text{fire}} = N_{\text{mem}} r_{\text{rep}}$. It then takes $T_{\text{com}} = L/c$ seconds, with $c$ the speed of light, for the photons to arrive on the ground, and another $T_{\text{com}}$ for the heralding signal to arrive back at the satellite. A full attempt of creating entanglement in one arm of the system thus takes $t_{\text{attempt}} = t_{\text{fire}} + 2T_{\text{com}}$. If we now create entanglement in one arm of the system, we must get entanglement in the other arm as well and swap the entanglement on the satellite to entangle the two ground stations. This procedure, however, needs to happen within a certain amount of tries, $N_{\text{max}}$, because otherwise the photons stored in the memories on the first arm will decohere or get lost from the memory. We could optimize the protocol to find the best cutoff time, but we choose a cutoff around half a coherence time for simplicity. The amount of attempts we can fit within this time $\tau/2$ is thus $N_{\text{max}} = \tau/2t_{\text{attempt}}$, rounded to an integer number of attempts. The coherence time that defines this window in which we look at the rate is that of the lowest coherence time of the four memories.
For the rate, we count all the possible ways of creating entanglement between Alice and Bob, by summing over the probabilities of establishing entanglement in arm $a$ in attempt $i$ and in arm $b$ in attempt $j$, where $i$ and $j$ are both limited by $N_{\text{max}}$. The probability of one photon, out of the $N_{\text{mem}}$ created, arriving at the receiver in one attempt is given by the probability of successfully creating an entangled pair on the satellite ($p_b p_w^2$), successfully transmitting it ($p_T$), and successfully heralding the photon upon arrival at the ground station ($\eta_{h,1}$) as[9]

$$p_e(t) = 1 - (1 - p_b p_w^2 p_T(t) \eta_{h,1})^{N_{\text{mem}}}. \tag{2.29}$$

After we have established entanglement in one arm with probability $p_e$, we still need to keep it until entanglement is formed in the other arm and we get the signal from the satellite with the outcome of the BSM. We lose a photon from the memory on the satellite with probability $1 - \mu_l$, after it was heralded with heralding efficiency $\eta_h$, and we lose a photon from the memory on the ground with probability $1 - \eta_l$. We also (optionally) herald the photon upon retrieval from the memory with efficiency $\eta_{h,2}$. We thus find the success probability for a coherence time starting at a time $t$, by summing over all

[9] This expression changes when dark counts are included, see Appendix A

possible ways of making entanglement between the ground stations as

$$\begin{aligned} p_{\text{succes}}(t) = \sum_{i=0}^{N_{\max}} \sum_{j\geq i}^{N_{\max}} \eta_{\text{BSM}} p_{e,a,i}\mu_{a,j-i}\eta_{a,j-i}\eta_h\eta_{h,2} \left[\prod_{k=0}^{i-1}(1-p_{e,a,k}\mu_{a,j-k}\eta_{a,j-k})\right] \\ p_{e,b,j}\mu_{b,1}\eta_{b,1}\left[\prod_{l=0}^{j-1}(1-p_{e,b,l}\mu_{b,1}\eta_{b,1})\right] \\ + \sum_{i=0}^{N_{\max}} \sum_{j>i}^{N_{\max}} \eta_{\text{BSM}} p_{e,a,j}\mu_{a,1}\eta_{a,1}\eta_h\eta_{h,2}\left[\prod_{k=0}^{j-1}(1-p_{e,a,k}\mu_{a,1}\eta_{a,1})\right] \\ p_{e,b,i}\mu_{b,j-i}\eta_{b,j-i}\left[\prod_{l=0}^{i-1}(1-p_{e,a,l}\mu_{b,j-l}\eta_{b,j-l})\right]. \end{aligned} \tag{2.30}$$

Where we used short-hand notations $p_{e,c,i} = p_{e,c}(t + it_{\text{attempt}}(t)); \mu_{c,i} = \mu_{l,c}(it_{\text{attempt}}(t)); \eta_{c,i} = \eta_{l,c}(it_{\text{attempt}}(t) - T_{\text{com}}(t))$, where the $l$ in $\mu_l$ or $\eta_l$, indicating that it is the memory efficiency dealing with losses, is omitted to avoid confusion with the summation index $l$. Note that one of the summations goes over $j \geq i$ and the other over $j > i$, to account for the case where we establish entanglement in both arms in one attempt.
Since $T_{\text{com}}$ depends on the distance between the satellite and the ground station, this changes over time, and thus $t_{\text{attempt}}$ and $N_{\max}$ as well. The start of one coherence-time window is called t, since the time window before a memory resets is rather short, and the link length will not change significantly in this window, we use this time to define other windows ($t_{\text{attempt}}$, $N_{\max}$, $T_{\text{com}}$) within this coherence time.
After each $N_{\max}$ attempts we reset all the memories and start over, $p_{\text{success}}(t)$ is thus the probability of having an entangled pair between the ground stations before a memory reset, which takes $N_{\max}t_{\text{attempt}}$ and starts at a time $t$. We then find the rate by multiplying our success probability by our reset rate as

$$\boxed{R(t) = \frac{p_{\text{success}}(t)}{(N_{\max}(t)t_{\text{attempt}}(t))}} \tag{2.31}$$

Note that this way of resetting the memory might not be the optimal way, since once entanglement between the two ground stations has been established we might want to start again and not wait until the end of the coherence time to try again. This way of calculating the rate also does not include the possibility of receiving more than one photon per attempt, or establishing entanglement in more than one pair between the ground stations in one coherence time. These simplifications are however justified for memories available now or in the near future since with current available technologies it will take in the order of 100 coherence times ($1/p_e\tau$) to entangle the ground stations, so the changes of this happening twice in one coherence time are small. And as transmission probability over larger distances are in the order of $10^{-6}$, we will not have enough memory modes on the satellite to have a reasonable probability of getting more than one photon to reach the ground station in one attempt. However, looking far into the future, where we might have quantum memories with millions of modes and minutes long coherence time, when this happens, the expression in Equation 2.30 will be oversimplified and will need to be adjusted, or should be taken as a lower bound.

### Fidelity

We can calculate the average fidelity of an arriving photon pair within a certain coherence time window by finding the fidelity of the state for each scenario we came across in Equation 2.30, namely having entanglement in one arm on attempt $i$, and in the other on attempt $j$. Now we turn to calculating the fidelity of the effective state that Alice and Bob share after they both received a photon and a swap has taken place in the satellite.
We start off looking at one arm of the system. On Alice's side, we start off with the state produced by the source in Equation 2.1, after which we apply the loss mode for loss from the source. We end up with

$$\rho_{\text{sat}}^{(a,A)} = p_{\text{suc}}\rho_\gamma + p_{\text{lose a}}|\varnothing\rangle\langle\varnothing| \otimes \text{Tr}_A(\rho_\gamma) + p_{\text{lose A}}\text{Tr}_a(\rho_\gamma) \otimes |\varnothing\rangle\langle\varnothing| + p_{\text{lose both}}|\varnothing\varnothing\rangle\langle\varnothing\varnothing|. \tag{2.32}$$

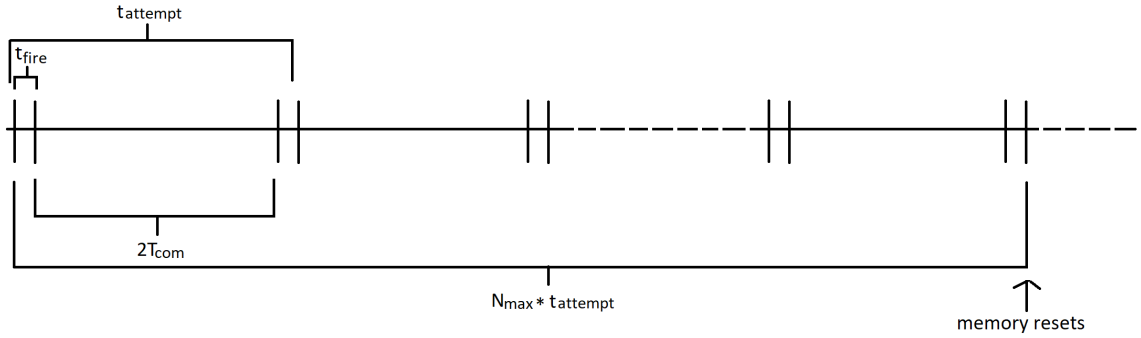


Figure 2.3: Visualisation of time windows relevant for calculating and defining the rate of the protocol. One attempt takes $t_{\text{attempt}}$, starts at time $t$ and consists of creating $N_{\text{mem}}$ entangled photon pairs in $t_{\text{fire}}$, then sending them to the receiver which takes $T_{\text{com}}$, and waiting for an heralding signal to arrive back which takes another $T_{\text{com}}$. The memories reset after $N_{\max}$ attempts.

With

$$\begin{aligned} p_{\text{suc}} &= p_b p_w^2, \\ p_{\text{lose a}} &= p_b(1-p_w)p_w = p_{\text{lose A}}, \\ p_{\text{lose both}} &= (1-p_b) + p_b(1-p_w)^2. \end{aligned} \tag{2.33}$$

One of these photons, the one in mode $a$, we will keep and store in a memory on the satellite. But first, it will be heralded. Since we assume that $p_{\text{suc}} \gg p_{\text{dark}}$ we neglect the dark counts in this step. We do apply a loss channel to deal with the heralding efficiency $\eta_h$ and then discard the vacuum terms in mode a and normalize the state:

$$\begin{aligned} \rho_{\text{sat}}^{(a,A)} \xrightarrow{\text{heralding efficiency}} \rho_{\text{herald}}^{(a,A)} =& p_{\text{suc}}\eta_h\rho_\gamma + \big(p_{\text{lose a}} + p_{\text{suc}}(1-\eta_h)\big)|\varnothing\rangle\langle\varnothing| \otimes \text{Tr}_A(\rho_\gamma) \\ &+ p_{\text{lose A}}\eta_h \text{Tr}_a(\rho_\gamma) \otimes |\varnothing\rangle\langle\varnothing| + \big(p_{\text{lose both}} + p_{\text{lose A}}(1-\eta_h)\big)|\varnothing\varnothing\rangle\langle\varnothing\varnothing| \\ \xrightarrow{\text{discard vacuum terms}} \rho_{\text{h}}^{(a,A)} =& p_{\text{suc}}\eta_h\rho_\gamma + p_{\text{lose A}}\eta_h \text{Tr}_a(\rho_\gamma) \otimes |\varnothing\rangle\langle\varnothing| \\ \xrightarrow{\text{normalize}} \rho_{h,n}^{(a,A)} =& \rho_{\text{h}}^{(a,A)} / \text{Tr}_a\left(\rho_h^{(a,A)}\right). \end{aligned} \tag{2.34}$$

Next, we load mode $a$ into the memory. We will use our memory channel from Equation 2.2 but replace $\eta \to \mu$ to distinguish this 'assisting' memory from the memory on the ground. For notational simplicity, we omit the time dependencies of $\mu_{a,l}$ and $\mu_{a,d}$.
While the qubit from mode $a$ is stored in a memory on the satellite for some time $t_a$, we will send the qubit from mode $A$ to the ground station. To model the transmission, we apply the loss channel with probability $p_{T,A}(t_e)$ at the time of emission to mode $A$. we find

$$\begin{aligned} \rho_{\text{transmitted}}^{(a,A)} =& A\rho_\gamma + B|\varnothing\rangle\langle\varnothing| \otimes \text{Tr}_a(\rho_\gamma) + C\text{Tr}_A(\rho_\gamma) \otimes |\varnothing\rangle\langle\varnothing| + D\text{Tr}_A(\rho_\gamma) \otimes \frac{\mathbb{1}}{2} \\ &+ E\frac{\mathbb{1}}{2} \otimes \text{Tr}_a(\rho_\gamma) + F\frac{\mathbb{1}}{2} \otimes \frac{\mathbb{1}}{2} + G|\varnothing\varnothing\rangle\langle\varnothing\varnothing| + H\frac{\mathbb{1}}{2} \otimes |\varnothing\rangle\langle\varnothing| + I|\varnothing\rangle\langle\varnothing| \otimes \frac{\mathbb{1}}{2}, \end{aligned} \tag{2.35}$$

with

$$
\begin{aligned}
A =& p_{\text{suc}}\eta_h\mu_{a,l}\mu_{a,d}p_{T,A}/\text{Tr}_a\left(\rho_{\text{h}}^{(a,A)}\right);\\
B =& p_{\text{suc}}\eta_h(1-\mu_{a,l})p_{T,A}/\text{Tr}_a\left(\rho_{\text{h}}^{(a,A)}\right);\\
C =& \left[p_{\text{lose A}}\eta_h\mu_{a,l}\mu_{a,d}+p_{\text{suc}}\eta_h\mu_{a,l}\mu_{a,d}(1-p_{T,A})\right]/\text{Tr}_a\left(\rho_{\text{h}}^{(a,A)}\right);\\
D =& 0;\\
E =& p_{\text{suc}}\eta_h\mu_{a,l}(1-\mu_{a,d})p_{T,A}/\text{Tr}_a\left(\rho_{\text{h}}^{(a,A)}\right);\\
F =& 0;\\
G =& \left[p_{\text{lose A}}\eta_h(1-\mu_{a,l})+p_{\text{suc}}\eta_h(1-\mu_{a,l})(1-p_{T,A})\right]/\text{Tr}_a\left(\rho_{\text{h}}^{(a,A)}\right);\\
H =& \left[p_{\text{lose A}}\eta_h\mu_{a,l}(1-\mu_{a,d})+p_{\text{suc}}\eta_h\mu_{a,l}(1-\mu_{a,d})(1-p_{T,A})\right]/\text{Tr}_a\left(\rho_{\text{h}}^{(a,A)}\right);\\
I =& 0.
\end{aligned}
\tag{2.36}
$$

Next up we herald the arrival of the photon from mode A before loading it into the memory on the ground. Since the transmission probability $p_T$ is going to be quite small, our dark count probability will be in the order of magnitude of the probability of a photon from the satellite arriving at the ground station, so we have to include the dark counts in this step. We get $\rho_{\text{transmitted}}^{(a,A)} \xrightarrow{\text{herald A}} \rho_{\text{t,h}}^{(a,A)}$, where the transmitted heralded state $\rho_{\text{t,h}}^{(a,A)}$ is the same as in Equation 2.35, but with primed coefficients given by

$$
\begin{aligned}
A' =& A\eta_h,\\
B' =& B\eta_h,\\
C' =& Cp_{\text{dark,v}} + A(1-\eta_h)p_{\text{dark,v}},\\
D' =& A(1-\eta_h)p_{\text{dark,d}} + Cp_{\text{dark,d}},\\
E' =& E\eta_h,\\
F' =& E(1-\eta_h)p_{\text{dark,d}},\\
G' =& B(1-\eta_h)p_{\text{dark,v}} + Gp_{\text{dark,v}},\\
H' =& E(1-\eta_h)p_{\text{dark,v}} + Hp_{\text{dark,v}},\\
I' =& B(1-\eta_h)p_{\text{dark,d}} + Gp_{\text{dark,d}}.
\end{aligned}
\tag{2.37}
$$

We can normalize our transmitted, heralded state as

$$
\rho_{\text{t,h,n}}^{(a,A)} = \rho_{\text{t,h}}^{(a,A)}/\text{Tr}_A\left(\rho_{\text{t,h}}^{(a,A)}\right). \tag{2.38}
$$

Our next step is to load mode A into the memory on the ground. This time we apply the memory channel on mode A, with memory efficiencies $\eta_{A,l}$ and $\eta_{A,d}$. We then find the state $\rho_{t,h,n}^{(a,A)\prime}$ with coefficients

$$
\begin{aligned}
A'' =& A'\eta_{A,l}\eta_{A,d}/\mathrm{Tr}_A\left(\rho_{\mathrm{t,h}}^{(a,A)}\right),\\
B'' =& B'\eta_{A,l}\eta_{A,d}/\mathrm{Tr}_A\left(\rho_{\mathrm{t,h}}^{(a,A)}\right),\\
C'' =& \left(C' + (A'+D')(1-\eta_{A,l})\right)/\mathrm{Tr}_A\left(\rho_{\mathrm{t,h}}^{(a,A)}\right),\\
D'' =& \left(D'\eta_{A,l} + A'\eta_{A,l}(1-\eta_{A,d})\right)/\mathrm{Tr}_A\left(\rho_{\mathrm{t,h}}^{(a,A)}\right),\\
E'' =& E'\eta_{A,l}\eta_{A,d}/\mathrm{Tr}_A\left(\rho_{\mathrm{t,h}}^{(a,A)}\right),\\
F'' =& \left(F'\eta_{A,l} + E'\eta_{A,l}(1-\eta_{A,d})\right)/\mathrm{Tr}_A\left(\rho_{\mathrm{t,h}}^{(a,A)}\right),\\
G'' =& \left(G' + (B'+I')(1-\eta_{A,l})\right)/\mathrm{Tr}_A\left(\rho_{\mathrm{t,h}}^{(a,A)}\right),\\
H'' =& \left(H' + (F'+E')(1-\eta_{A,l})\right)/\mathrm{Tr}_A\left(\rho_{\mathrm{t,h}}^{(a,A)}\right),\\
I'' =& \left(I'\eta_{A,l} + B'\eta_{A,l}(1-\eta_{A,d})\right)/\mathrm{Tr}_A\left(\rho_{\mathrm{t,h}}^{(a,A)}\right).
\end{aligned}
\tag{2.39}
$$

Lastly, when the heralding signal arrives at the satellite, the BSM is performed on modes $a$, $b$ of the joined system $\rho_{t,h,n}^{(a,A)\prime}\otimes\rho_{t,h,n}^{(b,B)\prime}$, which are the qubits stored in the memories on the satellite. This will swap the entanglement to create entanglement between the two qubits stored in the memories at the ground stations, like discussed in Section 2.1.5. If we lose any photons from the memory, we will see this in the click pattern of the BSM. Because of this, we can discard the vacuum terms in the $a$ and $b$ modes of Equation 2.39 and renormalize the state. We then find that

$$
\begin{aligned}
B'' &\to 0,\\
G'' &\to 0,\\
I'' &\to 0.
\end{aligned}
\tag{2.40}
$$

And we divide our terms by $\mathrm{Tr}_a(\rho_{t,h,n}^{(a,A)\prime})$.
In the BSM calculation, the terms in Table 2.1 are used.

| | $\lvert\langle\phi^+\rvert.\lvert\phi^+\rangle\rvert$ | $\lvert\langle\phi^-\rvert.\lvert\phi^-\rangle\rvert$ | $\lvert\langle\psi^+\rvert.\lvert\psi^+\rangle\rvert$ | $\lvert\langle\psi^-\rvert.\lvert\psi^-\rangle\rvert$ |
|---|---|---|---|---|
| $\rho_\gamma^{(a,b)}$ | $p_{\rho\rho}^{\phi^+} = p_0 + \frac{p_{\alpha\alpha}+p_{\beta\beta}}{2}$ | $p_{\rho\rho}^{\phi^-} = \frac{p_{\alpha\alpha}+p_{\beta\beta}}{2}$ | $p_{\rho\rho}^{\psi^+} = \frac{p_{\alpha\beta}+p_{\beta\alpha}}{2}$ | $p_{\rho\rho}^{\psi^-} = \frac{p_{\alpha\beta}+p_{\beta\alpha}}{2}$ |
| $\mathrm{Tr}_A(\rho_\gamma^{(a,A)})\otimes\frac{\mathbb{1}}{2}$ | $p_{\rho\frac{1}{2}}^{\phi^+} = \frac{p_0+p_{\alpha\alpha}+p_{\beta\beta}+p_{\alpha\beta}+p_{\beta\alpha}}{4}$ | $p_{\rho\frac{1}{2}}^{\phi^-} = \frac{p_{\alpha\alpha}+p_{\beta\beta}+p_{\alpha\beta}+p_{\beta\alpha}}{4}$ | $p_{\rho\frac{1}{2}}^{\psi^+} = \frac{p_0+p_{\alpha\alpha}+p_{\beta\beta}+p_{\alpha\beta}+p_{\beta\alpha}}{4}$ | $p_{\rho\frac{1}{2}}^{\psi^-} = \frac{p_{\alpha\alpha}+p_{\beta\beta}+p_{\alpha\beta}+p_{\beta\alpha}}{4}$ |
| $\frac{\mathbb{1}}{2}\otimes\mathrm{Tr}_B(\rho_\gamma^{(b,B)})$ | $p_{\rho\frac{1}{2}}^{\phi^+} = \frac{p_0+p_{\alpha\alpha}+p_{\beta\beta}+p_{\alpha\beta}+p_{\beta\alpha}}{4}$ | $p_{\rho\frac{1}{2}}^{\phi^-} = \lvert\frac{p_{\alpha\alpha}+p_{\beta\beta}+p_{\alpha\beta}+p_{\beta\alpha}}{4}$ | $p_{\rho\frac{1}{2}}^{\psi^+} = \frac{p_0+p_{\alpha\alpha}+p_{\beta\beta}+p_{\alpha\beta}+p_{\beta\alpha}}{4}$ | $p_{\frac{1}{2}\rho}^{\phi^-} = \frac{p_{\alpha\alpha}+p_{\beta\beta}+p_{\alpha\beta}+p_{\beta\alpha}}{4}$ |
| $\frac{\mathbb{1}}{2}\otimes\frac{\mathbb{1}}{2}$ | $p_{\frac{1}{2}\frac{1}{2}}^{\phi^+} = \frac{1}{4}$ | $p_{\frac{1}{2}\frac{1}{2}}^{\phi^-} = \frac{1}{4}$ | $p_{\frac{1}{2}\frac{1}{2}}^{\psi^+} = \frac{1}{4}$ | $p_{\frac{1}{2}\frac{1}{2}}^{\psi^-} = \frac{1}{4}$ |

Table 2.1: Some terms that are helpful in the calculation of the final state after the BSM. The overlap of state $xx$ (row) with Bell state $X$ (column) given by $p_{xx}^X$.

Our remaining state, after the BSM, is then

$$
\begin{aligned}
\rho_{t,h,n}^{(a,A)\prime}\otimes\rho_{t,h,n}^{(b,B)\prime}\to\rho_{\mathrm{mem}}^{(A,B)} =& p_{\mathrm{BSM}}\left(\eta^{\phi^+}\rho_{\phi^+} + \eta^{\phi^-}Z\rho_{\phi^-}Z + \eta^{\psi^+}X\rho_{\psi^+}X + \eta^{\psi^-}XZ\rho_{\psi^-}(XZ)^\dagger\right)\\
&+ (1-p_{\mathrm{BSM}})\frac{\mathbb{1}}{2}\otimes\frac{\mathbb{1}}{2},
\end{aligned}
\tag{2.41}
$$

Where $\eta^X$ are the probabilities of detecting the state $X$ in the BSM.
The states $\rho_X$ are given as

$$
\begin{aligned}
\rho_X =& A_X'''\rho_\gamma + B_X'''|\varnothing\rangle\langle\varnothing|\otimes\mathrm{Tr}_A(\rho_\gamma) + C_X'''\mathrm{Tr}_B(\rho_\gamma)\otimes|\varnothing\rangle\langle\varnothing| + D_X'''\mathrm{Tr}_B(\rho_\gamma)\otimes\frac{\mathbb{1}}{2}\\
&+ E_X'''\frac{\mathbb{1}}{2}\otimes\mathrm{Tr}_A(\rho_\gamma) + F_X'''\frac{\mathbb{1}}{2}\otimes\frac{\mathbb{1}}{2} + G_X'''|\varnothing\varnothing\rangle\langle\varnothing\varnothing| + H_X'''\frac{\mathbb{1}}{2}\otimes|\varnothing\rangle\langle\varnothing| + I_X'''|\varnothing\rangle\langle\varnothing|\otimes\frac{\mathbb{1}}{2},
\end{aligned}
\tag{2.42}
$$

with the terms ($p^X_{xx}$ as given in Table 2.1)

$$\begin{aligned}
A'''_X &= \left(p^X_{\rho\rho}A''_AA''_B + p^X_{\rho\frac{1}{2}}A''_AE''_B + p^X_{\frac{1}{2}\rho}E''_AA''_B + p^X_{\frac{1}{2}\frac{1}{2}}E''_AE''_B\right)/\mathrm{Tr}_a(\rho^{(a,A)\prime}_{t,h,n})\mathrm{Tr}_b(\rho^{(b,B)\prime}_{t,h,n}),\\
B'''_X &= \left(p^X_{\rho\rho}C''_AA''_B + p^X_{\rho\frac{1}{2}}C''_AE''_B + p^X_{\frac{1}{2}\rho}H''_AA''_B + p^X_{\frac{1}{2}\frac{1}{2}}{}''H_AE''_B\right)/\mathrm{Tr}_a(\rho^{(a,A)\prime}_{t,h,n})\mathrm{Tr}_b(\rho^{(b,B)\prime}_{t,h,n}),\\
C'''_X &= \left(p^X_{\rho\rho}A''_AC''_B + p^X_{\rho\frac{1}{2}}A''_AH''_B + p^X_{\frac{1}{2}\rho}E''_AC''_B + p^X_{\frac{1}{2}\frac{1}{2}}E''_AH''_B\right)/\mathrm{Tr}_a(\rho^{(a,A)\prime}_{t,h,n})\mathrm{Tr}_b(\rho^{(b,B)\prime}_{t,h,n}),\\
D'''_X &= \left(p^X_{\rho\rho}A''_AD''_B + p^X_{\rho\frac{1}{2}}A''_AF''_B + p^X_{\frac{1}{2}\rho}E''_AD''_B + p^X_{\frac{1}{2}\frac{1}{2}}E''_AF''_B\right)/\mathrm{Tr}_a(\rho^{(a,A)\prime}_{t,h,n})\mathrm{Tr}_b(\rho^{(b,B)\prime}_{t,h,n}),\\
E'''_X &= \left(p^X_{\rho\rho}D''_AA''_B + p^X_{\rho\frac{1}{2}}D''_AE''_B + p^X_{\frac{1}{2}\rho}F''_AA''_B + p^X_{\frac{1}{2}\frac{1}{2}}F''_AE''_B\right)/\mathrm{Tr}_a(\rho^{(a,A)\prime}_{t,h,n})\mathrm{Tr}_b(\rho^{(b,B)\prime}_{t,h,n}),\\
F'''_X &= \left(p^X_{\rho\rho}D''_AD''_B + p^X_{\rho\frac{1}{2}}D''_AF''_B + p^X_{\frac{1}{2}\rho}F''_AD''_B + p^X_{\frac{1}{2}\frac{1}{2}}F''_AF''_B\right)/\mathrm{Tr}_a(\rho^{(a,A)\prime}_{t,h,n})\mathrm{Tr}_b(\rho^{(b,B)\prime}_{t,h,n}),\\
G'''_X &= \left(p^X_{\rho\rho}C''_AC''_B + p^X_{\rho\frac{1}{2}}C''_AH''_B + p^X_{\frac{1}{2}\rho}H''_AC''_B + p^X_{\frac{1}{2}\frac{1}{2}}H''_AH''_B\right)/\mathrm{Tr}_a(\rho^{(a,A)\prime}_{t,h,n})\mathrm{Tr}_b(\rho^{(b,B)\prime}_{t,h,n}),\\
H'''_X &= \left(p^X_{\rho\rho}D''_AC''_B + p^X_{\rho\frac{1}{2}}D''_AH''_B + p^X_{\frac{1}{2}\rho}F''_AC''_B + p^X_{\frac{1}{2}\frac{1}{2}}F''_AH''_B\right)/\mathrm{Tr}_a(\rho^{(a,A)\prime}_{t,h,n})\mathrm{Tr}_b(\rho^{(b,B)\prime}_{t,h,n}),\\
I'''_X &= \left(p^X_{\rho\rho}C''_AD''_B + p^X_{\rho\frac{1}{2}}C''_AF''_B + p^X_{\frac{1}{2}\rho}H''_AD''_B + p^X_{\frac{1}{2}\frac{1}{2}}H''_AF''_B\right)/\mathrm{Tr}_a(\rho^{(a,A)\prime}_{t,h,n})\mathrm{Tr}_b(\rho^{(b,B)\prime}_{t,h,n}).
\end{aligned} \tag{2.43}$$

Just like in the previous scheme, we herald this state when taking it out of our memory before using it: we herald it with probability $\eta_{h,2}$ and neglect dark counts, so we again discard our vacuum terms. Our coefficients become

$$\begin{aligned}
A^{(4)}_X &= A'''_X\eta^2_{h,2},\\
B^{(4)}_X &= 0,\\
C^{(4)}_X &= 0,\\
D^{(4)}_X &= D'''_X\eta^2_{h,2},\\
E^{(4)}_X &= E'''_X\eta^2_{h,2},\\
F^{(4)}_X &= F'''_X\eta^2_{h,2},\\
G^{(4)}_X &= 0,\\
H^{(4)}_X &= 0,\\
I^{(4)}_X &= 0.
\end{aligned} \tag{2.44}$$

Our final state is then given by

$$\rho^{(A,B)}_{\mathrm{final}} = \rho^{(A,B)\prime}_{\mathrm{mem}}/\mathrm{Tr}\left(\rho^{(A,B)\prime}_{\mathrm{mem}}\right), \tag{2.45}$$

with $\rho^{(A,B)\prime}_{\mathrm{mem}}$ the state as given in Equation 2.41, but with

$$\rho_X \to \rho'_X = A^{(4)}_X\rho_\gamma + D^{(4)}_X\mathrm{Tr}_b(\rho_\gamma)\otimes\frac{\mathbb{1}}{2} + E^{(4)}_X\frac{\mathbb{1}}{2}\otimes\mathrm{Tr}_a(\rho_\gamma) + F^{(4)}_X\frac{\mathbb{1}}{2}\otimes\frac{\mathbb{1}}{2} \tag{2.46}$$

Lastly, we calculate the fidelity of this final state with respect to $|\phi^+\rangle$, which is given by $\langle\phi^+|\rho^{(A,B)\prime}_{\mathrm{final}}|\phi^+\rangle$, with $\rho^{(A,B)\prime}_{\mathrm{final}}$ given by Equation 2.45. We use

$$\begin{aligned}
\langle\phi^+|Z\rho Z^\dagger|\phi^+\rangle &= \langle\phi^-|\rho|\phi^-\rangle,\\
\langle\phi^+|X\rho X^\dagger|\phi^+\rangle &= \langle\psi^+|\rho|\psi^+\rangle,\\
\langle\phi^+|XZ\rho(XZ)^\dagger|\phi^+\rangle &= \langle\psi^-|\rho|\psi^-\rangle,
\end{aligned} \tag{2.47}$$

to find

$$f = \left\{\sum_{X\in[\phi^\pm,\psi^\pm]} p_{\mathrm{BSM}}\eta^X\left[p^X_{\rho\rho}A^{(4)}_X + p^X_{\rho\frac{1}{2}}D^{(4)}_X + p^X_{\frac{1}{2}\rho}E^{(4)}_X + p^X_{\frac{1}{2}\frac{1}{2}}F^{(4)}_X\right] + p^{\phi^+}_{\frac{1}{2}\frac{1}{2}}(1-p_{\mathrm{BSM}})\right\}/\mathrm{Tr}\left(\rho^{(A,B)\prime}_{\mathrm{mem}}\right). \tag{2.48}$$

Keep in mind that some of these terms depend on different times. We have the transmission probability at the time of emission, which may be different times for Alice's side of the system then for Bob. We also have the memory efficiencies, that depend on how long the photon is stored in that memory, for the four different memories in the scheme.
To find the average fidelity, we average over the fidelities of different possibilities of creating entanglement (in arm $a$ at attempt $i$ and in $b$ at attempt $j$: $f(t,i,j)$), weighted by their probabilities of occurring:

$$\begin{aligned} F(t) = \frac{1}{p_{\text{success}}(t)} \Bigg[ & \sum_{i=0}^{N_{\max}} \sum_{j \geq i}^{N_{\max}} \eta_{\text{BSM}} p_{e,a,i} \mu_{a,j-i} \eta_{a,j-i} \eta_h \eta_{h,2} \left( \prod_{k=0}^{i-1} (1 - p_{e,a,k} \mu_{a,j-k} \eta_{a,j-k}) \right) \\ & p_{e,b,j} \mu_{b,1} \eta_{b,1} \left( \prod_{l=0}^{j-1} (1 - p_{e,b,l} \mu_{b,1} \eta_{b,1}) \right) f_a(t,i,j) \\ & + \sum_{j=0}^{N_{\max}} \sum_{i>j}^{N_{\max}} \eta_{\text{BSM}} p_{e,a,i} \mu_{a,1} \eta_{a,1} \eta_h \eta_{h,2} \left( \prod_{k=0}^{i-1} (1 - p_{e,a,k} \mu_{a,1} \eta_{a,1}) \right) \\ & p_{e,b,j} \mu_{b,i-j} \eta_{b,i-j} \left( \prod_{l=0}^{j-1} (1 - p_{e,b,l} \mu_{b,i-l} \eta_{b,i-l}) \right) f_b(t,i,j) \Bigg] \end{aligned} \tag{2.49}$$

We use $f_a(t,i,j)$ if entanglement was formed in arm $a$ at attempt $i$ and arm $b$ at attempt $j$, with $j \leq i$ (entanglement was formed in arm $a$ first, or in both arms in the same attempt) and we use $f_b(t,i,j)$ when $i > j$ (entanglement was formed in arm $b$ first). We distinguish the cases where entanglement was created in arm $a$ first and when in $b$ first as this makes a difference in how long the modes will have been stored in each memory.
Just like in the previous scheme we can use the same equation but exclude the normalization and use the terms from Equation 2.43 instead of 2.44 if we do not include the last heralding step. We can still use Equation 2.49, but with

$$f = \sum_{X \in [\phi^\pm, \psi^\pm]} p_{\text{BSM}} \eta^X \left[ p^X_{\rho\rho} A'''_X + p^X_{\rho\frac{1}{2}} D'''_X + p^X_{\frac{1}{2}\rho} E'''_X + p^X_{\frac{1}{2}\frac{1}{2}} F'''_X \right] + p^{\phi^+}_{\frac{1}{2}\frac{1}{2}} (1 - p_{\text{BSM}}). \tag{2.50}$$

### 2.3.3 Memory assisted uplink

The derivation for the memory assisted uplink is very similar to that of the memory assisted downlink as we take the same steps (create entangled pairs, put half of them in the memory and send the other half to the receiver, when received swap entanglement). The differences are where theses steps take place (on the satellite or on the ground), on which modes the swap is performed and how long the photons need to be stored in the memories. There are also some differences in the parameters that are used. Fundamentally there will be a difference in transmission probability, but possibly also in hardware choices.
We have a slight advantage in storage time since we do not have to wait for the last heralding signal to perform the swap, as this is done at the receiver. This shortens the storage time of the photons at the satellite by $T_{\text{com}}$. With this, our rate has the same expression as in Equation 2.30, but now our notation convention changes to $p_{e,c,i} = p_{e,c}(t + it_{\text{attempt}}(t)); \mu_{c,i} = \mu_c(it_{\text{attempt}}(t) - T_{\text{com}}(t)); \eta_{c,i} = \eta_c(it_{\text{attempt}}(t) - 2T_{\text{com}}(t))$, where this time $\mu$ are for the memories on the ground and $\eta$ on the satellite. Up until the state in Equation 2.38, the calculations for the fidelity of the uplink scheme are the same as in the previous section. Then, we perform a BSM on modes $A$, $B$ (instead of $a$, $b$ like previously). This leads to the same states as in equations 2.41 and 2.42, except for $\rho^{(A,B)}_{\text{final}} \to \rho^{(a,b)}_{\text{final}}$ and with the

terms

$$
\begin{aligned}
A'''_X &= \left(p^X_{\rho\rho} A''_a A''_b + p^X_{\rho\frac{1}{2}} A''_a D''_b + p^X_{\frac{1}{2}\rho} D''_a A''_b + p^X_{\frac{1}{2}\frac{1}{2}} D''_a D''_b\right) / \mathrm{Tr}_A(\rho^{(a,A)\prime}_{t,h,n}) \mathrm{Tr}_B(\rho^{(b,B)\prime}_{t,h,n}),\\
B'''_X &= \left(p^X_{\rho\rho} B''_a A''_b + p^X_{\rho\frac{1}{2}} B''_a D''_b + p^X_{\frac{1}{2}\rho} I''_a A''_b + p^X_{\frac{1}{2}\frac{1}{2}} I''_a D''_b\right) / \mathrm{Tr}_A(\rho^{(a,A)\prime}_{t,h,n}) \mathrm{Tr}_B(\rho^{(b,B)\prime}_{t,h,n}),\\
C'''_X &= \left(p^X_{\rho\rho} A''_a B''_b + p^X_{\rho\frac{1}{2}} A''_a I''_b + p^X_{\frac{1}{2}\rho} D''_a B''_b + p^X_{\frac{1}{2}\frac{1}{2}} D''_a I''_b\right) / \mathrm{Tr}_A(\rho^{(a,A)\prime}_{t,h,n}) \mathrm{Tr}_B(\rho^{(b,B)\prime}_{t,h,n}),\\
D'''_X &= \left(p^X_{\rho\rho} A''_a E''_b + p^X_{\rho\frac{1}{2}} A''_a F''_b + p^X_{\frac{1}{2}\rho} D''_a E''_b + p^X_{\frac{1}{2}\frac{1}{2}} D''_a F''_b\right) / \mathrm{Tr}_A(\rho^{(a,A)\prime}_{t,h,n}) \mathrm{Tr}_B(\rho^{(b,B)\prime}_{t,h,n}),\\
E'''_X &= \left(p^X_{\rho\rho} E''_a A''_b + p^X_{\rho\frac{1}{2}} E''_a D''_b + p^X_{\frac{1}{2}\rho} F''_a A''_b + p^X_{\frac{1}{2}\frac{1}{2}} F''_a D''_b\right) / \mathrm{Tr}_A(\rho^{(a,A)\prime}_{t,h,n}) \mathrm{Tr}_B(\rho^{(b,B)\prime}_{t,h,n}),\\
F'''_X &= \left(p^X_{\rho\rho} E''_a E''_b + p^X_{\rho\frac{1}{2}} E''_a F''_b + p^X_{\frac{1}{2}\rho} F''_a E''_b + p^X_{\frac{1}{2}\frac{1}{2}} F''_a F''_b\right) / \mathrm{Tr}_A(\rho^{(a,A)\prime}_{t,h,n}) \mathrm{Tr}_B(\rho^{(b,B)\prime}_{t,h,n}),\\
G'''_X &= \left(p^X_{\rho\rho} B''_a B''_b + p^X_{\rho\frac{1}{2}} B''_a I''_b + p^X_{\frac{1}{2}\rho} I''_a B''_b + p^X_{\frac{1}{2}\frac{1}{2}} I''_a I''_b\right) / \mathrm{Tr}_A(\rho^{(a,A)\prime}_{t,h,n}) \mathrm{Tr}_B(\rho^{(b,B)\prime}_{t,h,n}),\\
H'''_X &= \left(p^X_{\rho\rho} E''_a B''_b + p^X_{\rho\frac{1}{2}} E''_a I''_b + p^X_{\frac{1}{2}\rho} F''_a B''_b + p^X_{\frac{1}{2}\frac{1}{2}} F''_a I''_b\right) / \mathrm{Tr}_A(\rho^{(a,A)\prime}_{t,h,n}) \mathrm{Tr}_B(\rho^{(b,B)\prime}_{t,h,n}),\\
I'''_X &= \left(p^X_{\rho\rho} B''_a E''_b + p^X_{\rho\frac{1}{2}} B''_a F''_b + p^X_{\frac{1}{2}\rho} I''_a E''_b + p^X_{\frac{1}{2}\frac{1}{2}} I''_a F''_b\right) / \mathrm{Tr}_A(\rho^{(a,A)\prime}_{t,h,n}) \mathrm{Tr}_B(\rho^{(b,B)\prime}_{t,h,n}).
\end{aligned}
\tag{2.51}
$$

The steps in Equations 2.44 through 2.50 are again the same. We can then also use the same averaging procedure to arrive at Equation 2.49:

$$
\begin{aligned}
F(t) = \frac{1}{p_{\text{success}}(t)} \Bigg[ &\sum_{i=0}^{N_{\max}} \sum_{j\geq i}^{N_{\max}} \eta_{\text{BSM}} p_{e,a,i} \mu_{a,j-i} \eta_{a,j-i} \eta_h \eta_{h,2} \left(\prod_{k=0}^{i-1} (1 - p_{e,a,k} \mu_{a,j-k} \eta_{a,j-k})\right)\\
&p_{e,b,j} \mu_{b,1} \eta_{b,1} \left(\prod_{l=0}^{j-1} (1 - p_{e,b,l} \mu_{b,1} \eta_{b,1})\right) f_a(t,i,j)\\
+ &\sum_{j=0}^{N_{\max}} \sum_{i>j}^{N_{\max}} \eta_{\text{BSM}} p_{e,a,i} \mu_{a,1} \eta_{a,1} \eta_h \eta_{h,2} \left(\prod_{k=0}^{i-1} (1 - p_{e,a,k} \mu_{a,1} \eta_{a,1})\right)\\
&p_{e,b,j} \mu_{b,i-j} \eta_{b,i-j} \left(\prod_{l=0}^{j-1} (1 - p_{e,b,l} \mu_{b,i-l} \eta_{b,i-l})\right) f_b(t,i,j) \Bigg]
\end{aligned}
$$

but with $p_{e,c,i} = p_{e,c}(t + it_{\text{attempt}}(t)); \mu_{c,i} = \mu_c(it_{\text{attempt}}(t) - T_{\text{com}}(t)); \eta_{c,i} = \eta_c(it_{\text{attempt}}(t) - 2T_{\text{com}}(t))$ and the terms from Equation 2.51.

## 2.4 Comparison to real world data

The direct downlink model is compared to data from the Micius satellite, which was used to distribute entangled photons between Delingha and Nanshan as reported in [43].

We first look at the transmission probability. We compare the measured data from supplementary material of [43] to our model for transmission probability by plotting the attenuation in dB over time during a fly-over in Figure 2.4. The attenuation is calculated as $-10\log_{10}(p_{T,a} p_{T,b})$, where $p_{T_a}$ and $p_{T,b}$ are the transmission probability for ground stations $a$ and $b$, as given by Equation 2.14. The most important parameters for our model are the positions of the ground stations and the satellite, which were reported. Some other parameters regarding hardware losses and weather conditions have been estimated. From Figure 2.4 we see that our model is in good agreement with the measured data, up to some fluctuations. These fluctuations could be caused by a change in weather conditions or some clouds. Another explanation for the deviations is the orbit of the satellite. The model assumes a circular orbit, but the actual orbit of the Micius satellite has an eccentricity of 0.0012. This is close to 0 (circular orbit), but the difference can account for small deviations.

Next, we compare the rate. The dark count probability $p_{\text{dark,d}} = 1.69 \cdot 10^{-5}$ is calculated as their reported dark count rate, divided by the source rate. With this we find an average entanglement distribution rate of 0.77 Hz, as can be seen as the horizontal line in Figure 2.5. This is a good approximation to their reported 1.1 Hz (8:1 signal to noise ratio). The difference may be explained

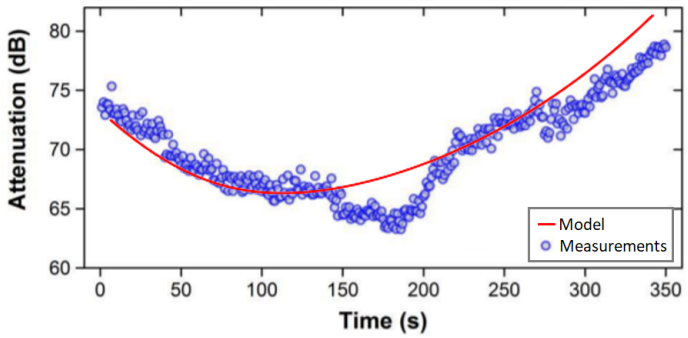


Figure 2.4: Comparison of our model for transmission probability (red) where attenuation in dB$=-10\log_{10}(p_{T,a}p_{T,b})$ compared to measured data for the Micius satellite (blue dots). The measured data are for a link between Delingha and Nanshan, as reported in the supplementary material of [43]. Besides some fluctuations in the measured data, due to fluctuations in weather or perhaps some clouds, we find that the model is in good agreement with measured data.

again by weather influences and not perfectly circular orbits as for the deviation in transmission probability described before. We also see in Figure 2.5 that the satellite enters the communication window around the same time every day, which is a result of the sun-synchronous orbit. With a source fidelity of 0.907 and an estimation of other parameters, we can also find good agreement in fidelity. The model gives an average fidelity of 0.89 of our output state, which is close to the reported 0.869±0.09 for the Delingha-Nanshan link.
Unfortunately, there is no data available to test the other schemes.

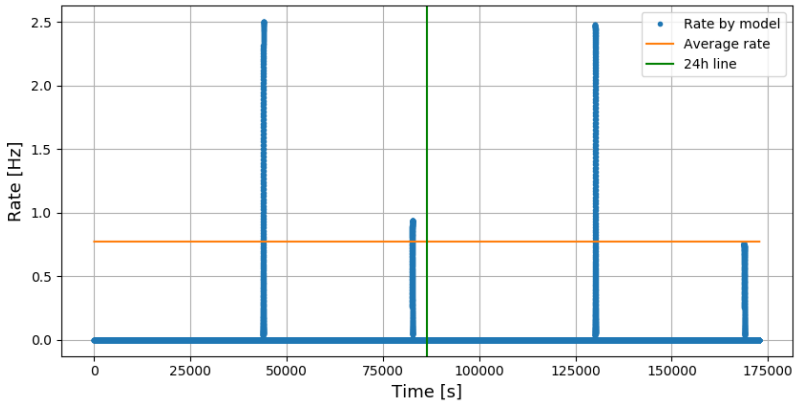


Figure 2.5: The rate of received entangled photon pairs between Delingha and Nanshan over 2 days, where the green vertical line separates the two days. The vertical blue lines consists of dots, which are data points of calculated rate every second, that make small parabolas for about 300 seconds as the satellite flies over. Most of the time, the satellite is not in the communication window, so the rate is zero. We see that the satellite enters the communication window around the same time every day, which is a result of the orbit being sun-synchronous. The average rate of 0.77 Hz is indicated by the horizontal orange line which is a good approximations of the 1.1 Hz (8:1 signal to noise ratio) reported in [43].

# Chapter 3

# Results, discussion and conclusion

In this chapter we will put our model to work. Our aim is to show the power of the model by applying it to different scenarios, as well as to give some interesting insights. First we identify a set of state-of-the-art parameters to see how well we can do with currently or near-term available hardware. Next, we identify a set of parameters to improve on, and see what this will mean for our rate and fidelity. Our model has many different parameters to play around with. Here, we look at changing parameters to optimize the rate and fidelity separately. We are also mostly focused on just changing small sets of parameters at a time, while keeping the rest the same. There are endless combinations of parameters that can be made which are beyond the scope of this project.

## 3.1 State of the art parameters, benchmark

The numbers reported here serve as a benchmark. In all following calculations we will use the parameters from this benchmark unless stated otherwise. For each parameter separately, we looked at recent and popular papers who report on them for each part of the setup. For the memory parameters, for example, we look specifically for memories with high multimode capacity to get $N_{\text{mem}}$ and separately for memories with long coherence times to find $\tau$. In reality it may not always be possible to combine these parameters into one setup, but it is good to see where this set of parameters might bring us in the future. We again refer to the list of variables in the beginning of the thesis to remind the reader of the meaning of the parameters.

**Entangled photon pair source:**

- $r_{\text{rep}} = 10$MHz based on a quantum dot source [44];
- $p_b$=0.8 ($p_w = 1$) [44];
- $p_0 = 0.972$, $p_{\alpha\alpha} = 0.008$, (estimation from figure:)$p_{\alpha\beta} = p_{\beta\alpha} = 0.005$ Figure 3 of [45] encoding: $\alpha = \text{H}$; $\beta = \text{V}$.

**Heralding:**

- $p_{\text{dark,d}} = 0$, $p_{\text{dark,v}} = 10^{-6}$ (estimate);
- $\eta_h = 0.5$ [46].

**Memory:**

- $N_{\text{mem}} = 100$ based on an atomic frequency comb memory [47];
- $\tau = 1$s based on nuclear spin based memory [26];
- $\eta_d' = 0.994$ [48];
- $\eta_l' = 0.9$ [49].

**BSM:**

- F=0.90 $\rightarrow p_{\text{BSM}} = 0.87$ [50];
- $\eta^{\phi^+}$=0.82; $\eta^{\phi^-}$=0.07; $\eta^{\psi^+}$=0.09; $\eta^{\psi^-}$=0.02 [31];
- $\eta_{\text{BSM}} = 0.89$ [31].

**Transmission:**

- $w_0 = 0.0308$ m, based on supplementary material of [42];
- $L_p$=2 dB; $L_T = L_j = L_R$ =1 dB based on estimations and [42];
- $\tau_0 = -\log(Tr)$, Tr = atmospheric transmittance = 0.98, based on MODTRAN simulations, for example in [51].

**Satellite orbit and ground stations:**

- $\alpha = 1.699$ rad (near-polar);
- Delft = 4.37° longitude, 51.99° latitude;
- Delft-Houston link: h = 6000 km, Houston = -95.36° longitude, 29.75° latitude;
- Delft-Paris link: h = 800 km, Paris = 2.29° longitude, 48.85° latitude;
- Receiver radius ground station: 0.6 m, satellite receiver radius: 0.2 m.

We have chosen to look at a Delft-Houston link for intercontinental connections, and a Delft-Paris link for international connections. The choice in ground station positions are otherwise quite arbitrary. The satellite orbit heights are chosen to have a good balance between the length of the communication window and the transmission probability, but are not fully optimized.

This set of parameters is a bit ambitious, but as we will see in the rest of this chapter, we have to be ambitious to receive a usable rate and fidelity.
Now that we have our set of benchmark parameters, we will see what this gives us in terms of rate and fidelity, and then see where we need to focus improvements on to make a usable link.

## 3.2 Rate

One of the main parameters to be considered in quantum communication is the rate, the speed at which we can receive entangled photon pairs. The high losses in fibres, greatly reducing the rate of the protocol, is what lead us to space-based segments to begin with. Here we will see how the rate behaves as the satellite flies over the ground stations. Then we explore what parameter improvements are most effective to improve the achievable rate.
The dependency of time, the dynamic link tracking and asymmetry as well as a model for transmission probability that is dependent on the links, is an important aspect of our model. To show this dynamic behavior, the rate over a typical flyover with the benchmark parameters, and a coherence time of $\tau = 0.5$s are plotted in Figures 3.1a-3.1c for all schemes. We see that the rate peaks around the middle of the flyover. The peak occurs here because the distance between the satellite and the ground station is shortest here, which gives the highest transmission probability. The transmission probability is given by Equation 2.14. We also see some interesting behavior where the rate makes a jump at two points in time for the memory assisted schemes, this can be explained by our memory reset protocol. We reset the memories after $N_{\text{max}}$ attempts, which is an integer. How many attempts fit within this $N_{\text{max}}$ is determined by how many attempts fit in half a coherence time, but as the link length changes, so does $t_{\text{attempt}}$. Initially, 5 attempts fit in half a coherence time before the memories reset, the jumps occur when the link becomes short enough to fit in one extra attempt before the memory resets, or one less in the second jump.

In a direct downlink, there are not many things we can do to increase the rate of the protocol. The major parameter to increase the rate of the protocol would be the source rate. However, a factor 10

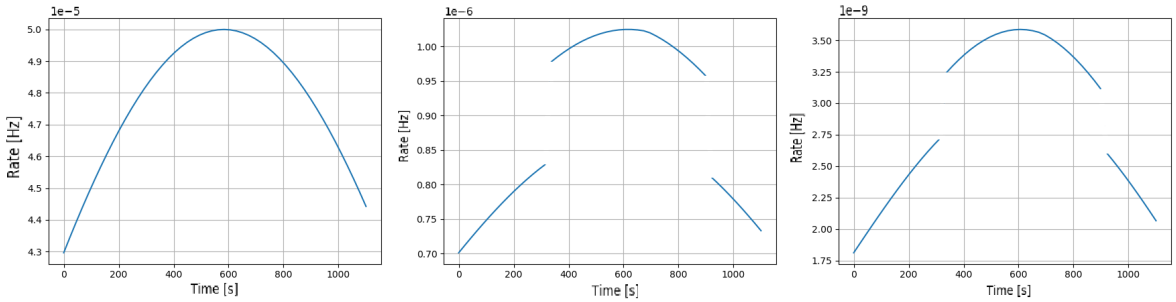


(a) Direct downlink (b) Memory assisted downlink (c) Memory assisted uplink

Figure 3.1: Rate over time for a typical flyover in a Delft-Houston link, to show the dynamic element of our model. The rate peaks at a rate of about $5 \cdot 10^{-5}$ Hz for the direct downlink (a), $1.1 \cdot 10^{-6}$ Hz for the memory assisted downlink (b) and $3.6 \cdot 10^{-9}$ Hz for the memory assisted uplink (c). This happens where the total link length is shortest, which is when the satellite is more or less in the middle of the two ground stations, seen here at around 600 seconds. The jumps at around 300 and 900 seconds in the memory assisted schemes occur due to a change in $N_{\max}$, the jumps are not seen in the direct downlink as we do not have the memory reset protocol here. From this figure we see interesting effects of the dynamic element of our model.

increase in your source rate will only lead to a factor 10 increase in your rate, so we can not expect to increase the rate by a lot here. Increasing the coherence time of your memories, such that we have a low chance of losing it while the results are communicated, can also increase the rate. However, once we are past a coherence time where we can relatively safely store our photons for the communication time $T_{\text{gcom}}$, this will only influence the rate by a small factor. Lastly, having a few more memory slots at your receiving memory can help for the case where a second photon arrives before we have communicated the results of a photon that arrived earlier. But as we see in Figure 3.2 about 10 memory slots will be more than enough to catch all incoming photons ($p_a \approx 1$), after that increasing the amount of memory slots won't affect the rate.

For the memory assisted schemes changing the source rate will not have a very big effect, as it will merely slightly decrease the time to make the photon pairs $t_{\text{fire}}$ and thereby the time it takes to complete one attempt $t_{\text{attempt}}$. However, increasing the amount of memory slots will have a big impact. More memory slots means that we create, and send down or up, more photons per attempt, and thereby increasing the probability of creating entanglement in an arm per attempt. A photon will then spend less time on average in the memory, and we will need fewer attempts to have entanglement between our ground stations. In Figure 3.2 we see that increasing the amount of memory slots by one order of magnitude can lead to an increase in rate by about 2 orders of magnitude. However, after about $10^5$ memory slots in the long Delft-Houston link and $10^3$ in the shorter Delft-Paris link, we see some saturating behavior at the top right parts of Figures 3.2a and 3.2b. This behavior is partly due to a fundamental limit, where our rate will always be limited by our source rate times the transmission probability (or transmission probability squared for the direct downlink), but also an artificial effect of how the protocol is set up. Increasing the amount of memory slots by that much will lead to a large $t_{\text{fire}}$. We will also have a pretty high probability of creating entanglement in one arm within one attempt. At this point, creating your $N_{\text{mem}}$ photons, sending them to the receiver, waiting for a result (the routine as outlined in Section 2.3.2) does not make sense. It would make more sense to adopt a protocol more similar to the direct downlink, where the photons are sent to the receiver continuously. This way, the rate may be higher then reported in these regimes, but again limited by $r_{\text{rep}} p_T$.

Again we see that increasing the memory coherence time does not affect the rate a lot, but it does have a bigger effect in the memory assisted schemes than on the direct downlink. This is because a higher coherence time will lead to an increase in $N_{\max}$, so we can try to create entanglement in more attempts before the memories reset.

From the comparison in Figure 3.2a and 3.2b, which shows the entanglement distribution rate for different scenarios, we see that the memory assisted schemes might outperform the direct downlink in future settings, especially when quantum memories become very well developed, and we want to create very long (intercontinental) links, like the Delft-Houston link. The uplink has a lower rate than

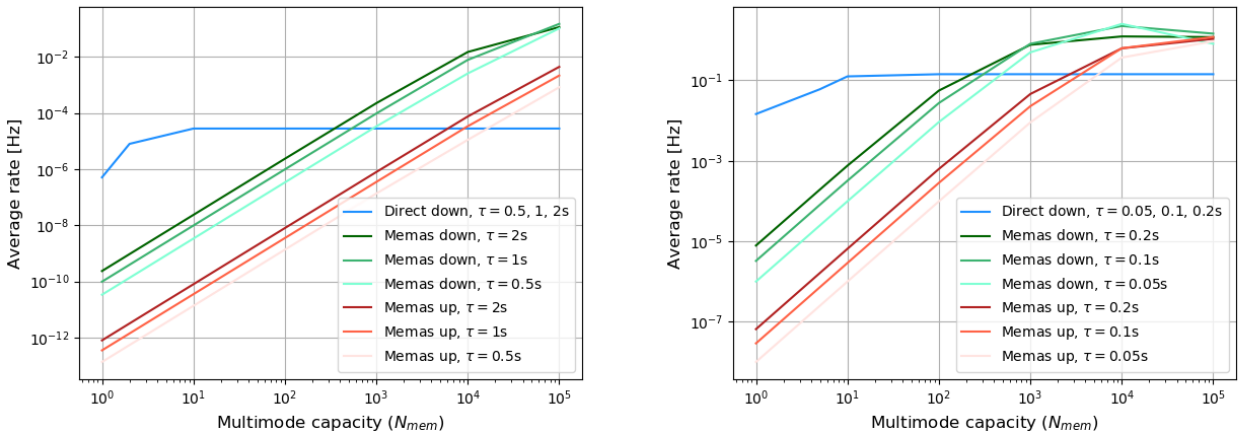


(a) Delft-Houston link

(b) Delft-Paris link

Figure 3.2: Rate of received entangled photon pairs, calculated with the benchmark parameters outlined in Section 3.1, with varying memory multimode capacity $N_{\text{mem}}$ and memory coherence time $\tau$, for a direct downlink (blue), memory assisted downlink (green) and memory assisted uplink (red). There is only one blue line, as the outcomes for coherence times of 0.5, 1 and 2 seconds give approximately the same outcome for the direct downlink, such that the lines lie on top of each other. For the Delft-Houston link (a), the memory assisted downlink outperforms the direct downlink with more than a few hundred memory slots. The memory assisted uplink will need up to ten thousand memory slots to outperform the direct downlink. For the Delft-Paris link (b) the crossover happens around a few thousand and a few tens of thousands for the down- and uplink, respectively. Each line is made up off 7 data points, where each data point is the rate averaged over 10 points in time during one flyover. This figure thus tells us which scheme is most favourable for a certain number of memory modes. We find that we will need the memory assisted schemes with a high multimode capacity for long intercontinental links.

the downlink, a big difference in this is that the receiver is assumed to be smaller for the uplink (0.2 m) than for the downlink (0.6 m). This was chosen because it is more difficult to put a big receiver on a satellite, but with this, we also need to give the uplink some credit. If we are limited in size with what we put on the satellite, then scaling in multimode capacity is a lot easier for the uplink, where the assisting memory is located at the ground stations.
One parameter that we have not discussed in this section is the transmission probability. We do have some control over this parameter and we will see how we can improve this in the next section.

## 3.3 Transmission probability and receiver radius

The transmission of the photon from the emitter to the receiver is by far the biggest source of loss, as the transmission probability = 1-loss probability, for the Delft-Houston link is in the order of $10^{-5}$ for downlinks (direct or memory assisted) and $10^{-6}$ for uplinks[1], where other sources of loss like from the memory or non-efficient heralding are around 0.5. Therefore, we would like to minimize the transmission loss as much as possible. The parameters that we can have control over are the beam waist $w_0$, the wavelength $\lambda$ of the signal, the hardware losses $L_p, L_T, L_R, L_j$ (to some degree) and the radius of the receiver aperture.
The choice of wavelength will depend, amongst other things, on the atmospheric transmittance at that wavelength. Common choices are around 850 nm or 1550 nm, where in this thesis 1550 nm was used for all calculations[2].

[1]Though this is a big source of loss, it is much better compared to fibre transmission, where a direct fibre link between Delft and Houston would lead to a transmission probability of about $10^{-240}$.

[2]This choice was made after consulting assistant professor R. Saathof from the space systems engineering department of TU Delft. At 1550 nm, we have relatively low background radiation, good atmospheric transmittance and a good

The hardware losses can be minimized, but not much improvement can be made here, as a lot of research on this area has been done for classical systems, similar for the beam waist.
There is also a choice in using an uplink or a downlink. Uplink losses will generally be higher because of the initial boost in beam spreading due to the atmosphere. This does not affect the downlink so much as the downlink only enters the atmosphere at the very last bit of its journey. This effect can be seen by looking at Equations 2.9 and 2.10, which describe the effect of the atmosphere on beam spreading. The index structure constant $C_n^2$ is higher close to the earth's surface and decreases rapidly with height, this can be seen in Equation 2.11 as well Figure 2.2 where it is plotted. In $T_{\text{up}}$ the factor $1-(h-h_0)/L$ is largest close to the ground station, where $C_n^2$ is also large. For the downlink, we have a factor $(h-h_0)/L$, which is smallest where $C_n^2$ is largest. From this we find that an uplink beam has more atmospheric induced spreading than the downlink, which leads to higher losses.
A parameter that can make a big difference in transmission probability is the radius of the receiver aperture. This determines how much of the signal is picked up. How the transmission probability changes with receiver radius for up- and downlinks can be found in Figure 3.3. We see that indeed the losses for an uplink are always a bit higher than for a downlink with comparable receiver radii, stemming from the atmosphere problem described before. An extra factor in why uplink losses are generally higher than downlink losses has to do with the placement of the receiver. For an uplink, the receiver is located on the satellite, where it can be much more challenging to increase the size of your equipment compared to a receiver on the ground. For this reason, the benchmark parameters are chosen as 0.2 m for the receiver on the satellite and 0.6m for the receiver at the ground stations. There is probably some room for improvement here, since certain equipment that will need to be on the satellite for the quantum memories and BSM will likely also be quite large.
From Figure 3.3 we also see that we can have a factor 10 increase in transmission probability if we increase the receiver radius from the benchmark of 0.6 meters to 1.9 meters in the downlink, or from 0.2 meters 0.7 meters for the uplink.
As a comparison, the effective beam width (Equation 2.8) after travelling the whole link length for a Delft-Houston link will be around 40 kilometers for an uplink and 17 kilometers for a downlink, so we can never make a receiver big enough to pick up the whole signal.
So to conclude, the largest impact on minimizing the transmission losses can be made by increasing the size of the receiver. Choosing a downlink instead of an uplink will also reduce losses, but this will not only impact the losses as it changes the whole protocol.

## 3.4 Fidelity

Now that we have identified the main parameters to improve on to increase the rate of the protocol, we will now do a similar analysis for the fidelity.
The fidelity of the final entangled pairs is determined by the fidelity of the created entangled pairs from the source, the dark counts and the decoherence of the state before use. The decoherence can take place in the memories (increased probability of decoherence over storage time) or from the entanglement swap.
With our benchmark parameters, we find that we can get a good fidelity for the direct downlink, about 0.91 on average. Unfortunately things do not look so bright for the memory assisted schemes, where we find 0.46 for the memory assisted downlink and 0.50 for the uplink. To identify what the main cause of this low fidelity is, we set each part of the protocol to 'perfect' one by one and see how much higher the output fidelity is compared to the benchmark case. The results of this can be seen in figure 3.4, where we have plotted the difference between the benchmark fidelity and the fidelity with one perfect component for all schemes. We see that the entanglement swap has the biggest effect on the fidelity in the memory assisted schemes. As the direct downlink does not have an entanglement swap in the protocol, this of course does not affect its fidelity. We can improve on all schemes by improving the memory and source, although these parameters are already quite good in the benchmark.

One of the reasons the fidelity is so greatly impacted by the entanglement swap is because there has been less advancement on this level: the best sources output pretty high fidelity, the dark counts are low and the memories are cut off before too much decoherence happens, but the entanglement swapping and teleportation protocols are not this advanced. There is a lot of improvement possible, specifically for the parameter $p_{\text{BSM}}$. To see how improving $p_{\text{BSM}}$ affects average fidelity, we refer to

balance between the Rayleigh scattering and infrared absorption.

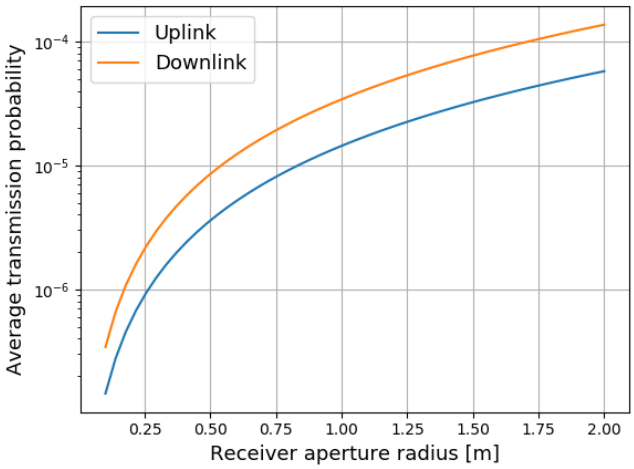


Figure 3.3: Transmission probability averaged over one flyover for a Delft-Houston link, over varied receiver aperture radii for up- and downlink. The downlink has higher transmission probability than the uplink for the same receiver radii. The receiver will also likely be larger in a downlink because we can keep it on the ground instead of having to put it on a satellite as for the uplink. We do see that we can improve our transmission probability by about a factor of 10 in the downlink from our benchmark of 0.6 m to 2 m. If we increase the size of the receiver on the satellite in the uplink from the benchmark of 0.2 m to 0.5 m, that will also give us about a factor 10 increase in transmission probability. This figure thus shows the high impact of increasing the receiver aperture radius.

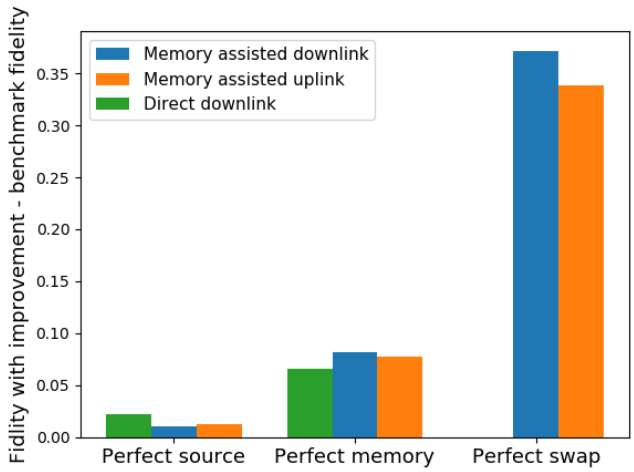


Figure 3.4: The impact (output fidelity - benchmark fidelity) making a certain part of the protocol perfect has on the fidelity compared to benchmark parameters for a Delft-Houston link. Plotted for a direct downlink (green), memory assisted downlink (blue) and memory assisted uplink (orange). We see that having a perfect memory will increase the fidelity for all schemes, a bit more than having a source that emits perfect Bell states. The most improvement on the fidelity can be made by doing a better entanglement swap, but only for the memory assisted schemes as the direct scheme does not have a swap.

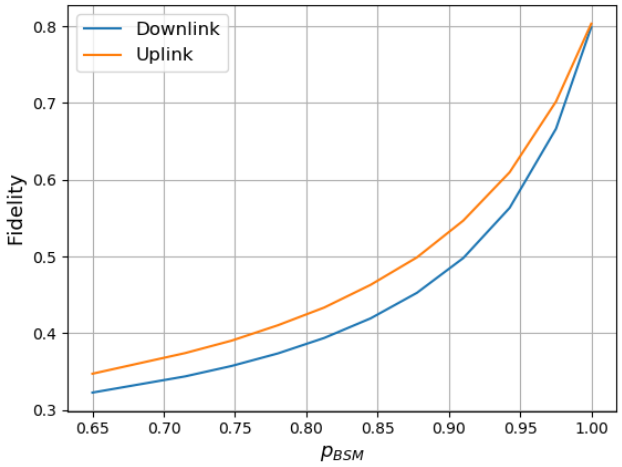


Figure 3.5: Average output fidelity of Delft-Houston link with varying qualities of entanglement swapping, ranging from 0.65 to perfect (1). Shown for both up- and downlink. We see that we can increase the fidelity by more then 0.3 by improving our benchmark $p_{\text{BSM}}$ of 0.86 to 1 and conclude that this is an important parameter to focus improvement on.

Figure 3.5, which shows the (average) output fidelity of a protocol where the entanglement swapping gets better by improving $p_{\text{BSM}}$ until it is perfect. There we see that we we can improve our fidelity from about 0.5 to about 0.8 if we had a perfect entanglement swap, compared to the benchmark.

## 3.5 Conclusion

With current available technologies, the direct downlink scheme applied to shorter (not intercontinental) links, is the only option. The two main limitations on the memory assisting schemes outperforming the direct downlink scheme are in the multimode capacity of the assisting memory and the quality of the entanglement swap.
The direct downlink will always outperform the memory assisted schemes in terms of fidelity, but increasing the entanglement swap quality to have $p_{\text{BSM}}$ above 0.98, we can achieve a fidelity around 0.70 for the uplink, and around 0.66 for the downlink, which can be seen in Figure 3.5. While this is still not great, we also have some room for improvement in the decoherence in the quantum memories.
In our intercontinental Delft-Houston link scenario, the direct downlink scheme has an average rate of about $3 \cdot 10^{-5}$ Hz. With an average fly-over lasting about 1100 seconds, we will effectively not be able to establish an entanglement link in this setup. We can reach a rate where we can expect to receive more than one entangled pair per flyover in the memory assisted schemes, for a few thousand memory modes in the downlink or several tens of thousands for the uplink, as can be seen in Figure 3.2. The memory assisted schemes will outperform the direct downlink in terms of rate if we can have a multimode capacity of more than about a few hundred memory slots for the downlink, or about ten thousand memory slots for the uplink, when all other parameters adhere to the benchmark as outlined in Section 3.1.
We also find that we can limit the transmission losses by scaling up the size of the receiver aperture, so we can 'catch' as much of the signal as possible. If we were able to use the same receiver aperture radius for the Delft-Houston uplink as for the downlink, then the average transmission probability will increase by almost one order of magnitude (a factor of 9) with respect to the benchmark. To increase the average transmission probability for a downlink by one order of magnitude with respect to the benchmark (0.6 m receiver radius), we will need a receiver that has a radius of about 1.9 meters.
From the results shown before it may seem easy to discard the uplink as a contender as the rate is quite a bit lower for the uplink than for the downlink and the fidelity is only a bit higher. However, uplinks may have an advantage in construction, having the more complicated equipment on the ground instead of on the satellite. Another point in favour of the uplink is that the lower rate is also partially

from the assumption of having a smaller receiver radius, which is not a fundamental limitation. If there is a strict limitation on the size of the satellite, this would also hinder the downlink, as scaling up orders of magnitudes in the available memory modes will likely also involve big hardware.
For shorter links, like the Delft-Paris link, we can achieve a good-enough rate with the direct downlink. For this reason, we are less likely to need the memory assisted schemes.

## 3.6 Outlook

Here I have focused on single links, but eventually, to obtain a global network ('quantum internet') we might need a network of quantum satellites. Within QuTech, researchers are working on extending the idea of using quantum satellites. Vicky Dominguez Tubio is working on using satellites as relay stations, as well as finding ways to optimize the satellite path.
It might be interesting to extend the model to be suitable for higher multimode capacities in the memory assisted schemes, where the protocol is not so clearly cut into attempts and more resembles the direct scheme. There might be a way of including the parameter $p_a$, which gives the probability that there is space in the memory for the incoming photon to be stored and is used in the direct downlink scheme, in a new expression for the memory assisted schemes.
It is also interesting to see how the rate is affected by changing the path of the satellite or the positions of the ground stations: what is the optimal way for the satellite to pass the ground stations? We can use such questions in choosing how to set up a global quantum network.

# Appendices

# Appendix A

# Rate including dark counts

If we want to be more precise, we include the dark counts that are stored as a maximally mixed state into the rate. In the main portion of the thesis this was left out because generally $p_{\text{dark}} \ll 1$ and it makes the expressions a bit more lengthy. We include them here for the sake of completeness.
The rate for the direct downlink scheme, given by Equation 2.15, goes like the success probability of the full scheme multiplied by the repetition rate. If we now include the dark counts, we will have a situation where something went wrong but we didn't know because we had a dark count. This will lead to a (slightly) higher rate, although lower fidelity. The expression can be written as

$$R = r_{\text{rep}} \Big[ p_b p_w^2 p_{T,a} p_{T,b} \eta_{h,1}^2 + p_b p_w p_{T,a} \eta_{h,1} (1 - p_w p_{T,b} \eta_{h,1}) p_{\text{dark,d}} + p_b (1 - p_w p_{T,a} \eta_{h,1}) p_w p_{T,b} \eta_{h,1} p_{\text{dark,d}} + \big[ (1 - p_b) + p_b (1 - p_w p_{T,a} \eta_{h,1})(1 - p_w p_{T,b} \eta_{h,1}) \big] p_{\text{dark,d}}^2 \Big] p_{a,a} p_{a,b} \eta_{a,l}(t) \eta_{b,l}(t) \eta_{h,2}^2 \tag{A.1}$$

Similarly for the memory assisted schemes. The parameter $p_e$ from Equation 2.29 will become

$$p_{e,c}(t) = 1 - \big(1 - p_b p_w p_{T,c} \eta_{h,1} - (1 - p_b p_w p_{T,c} \eta_{h,1}) p_{\text{dark,d}}\big)^{N_{\text{mem}}} \tag{A.2}$$

($c \in [a, b]$) This takes into account the possible dark counts before loading the state into the memory.

# Bibliography


[1] Erwin Schrödinger. Die gegenwärtige situation in der quantenmechanik. *Naturwissenschaften*, 23(49):823–828, 1935.

[2] Robert Raussendorf and Hans J Briegel. A one-way quantum computer. *Physical Review Letters*, 86(22):5188, 2001.

[3] Charles H Bennett and Stephen J Wiesner. Communication via one-and two-particle operators on einstein-podolsky-rosen states. *Physical review letters*, 69(20):2881, 1992.

[4] Gui-lu Long, Fu-guo Deng, Chuan Wang, Xi-han Li, Kai Wen, and Wan-ying Wang. Quantum secure direct communication and deterministic secure quantum communication. *Frontiers of Physics in China*, 2(3):251–272, 2007.

[5] Corning Incorporated.

[6] H-J Briegel, Wolfgang Dür, Juan I Cirac, and Peter Zoller. Quantum repeaters: the role of imperfect local operations in quantum communication. *Physical Review Letters*, 81(26):5932, 1998.

[7] Sheng-Kai Liao, Wen-Qi Cai, Wei-Yue Liu, Liang Zhang, Yang Li, Ji-Gang Ren, Juan Yin, Qi Shen, Yuan Cao, Zheng-Ping Li, et al. Satellite-to-ground quantum key distribution. *Nature*, 549(7670):43–47, 2017.

[8] Anton Lauenborg Andersen. Quantum key distribution and entanglement distribution with satellite links. Master's thesis, University of Copenhagen, 2020.

[9] John S Bell. On the einstein podolsky rosen paradox. *Physics Physique Fizika*, 1(3):195, 1964.

[10] A. Einstein, B. Podolsky, and N. Rosen. Can quantum-mechanical description of physical reality be considered complete? *Phys. Rev.*, 47:777–780, May 1935.

[11] Paul Adrien Maurice Dirac et al. *The principles of quantum mechanics*. Number 27. Oxford university press, 1981.

[12] H.-J. Briegel, W. Dür, J. I. Cirac, and P. Zoller. Quantum repeaters: The role of imperfect local operations in quantum communication. *Phys. Rev. Lett.*, 81:5932–5935, Dec 1998.

[13] Markus Aspelmeyer, Thomas Jennewein, Martin Pfennigbauer, Walter R Leeb, and Anton Zeilinger. Long-distance quantum communication with entangled photons using satellites. *IEEE Journal of Selected Topics in Quantum Electronics*, 9(6):1541–1551, 2003.

[14] Charles H Bennett and Gilles Brassard. Quantum cryptography: Public key distribution and coin tossing. *arXiv preprint arXiv:2003.06557*, 2020.

[15] Artur K. Ekert. Quantum cryptography based on bell's theorem. *Phys. Rev. Lett.*, 67:661–663, Aug 1991.

[16] Anne Broadbent, Joseph Fitzsimons, and Elham Kashefi. Universal blind quantum computation. In *2009 50th Annual IEEE Symposium on Foundations of Computer Science*, pages 517–526. IEEE, 2009.

[17] Vittorio Giovannetti, Seth Lloyd, and Lorenzo Maccone. Quantum-enhanced measurements: beating the standard quantum limit. *Science*, 306(5700):1330–1336, 2004.

[18] Ebubechukwu O Ilo-Okeke, Louis Tessler, Jonathan P Dowling, and Tim Byrnes. Remote quantum clock synchronization without synchronized clocks. *npj Quantum Information*, 4(1):1–5, 2018.

[19] David C Burnham and Donald L Weinberg. Observation of simultaneity in parametric production of optical photon pairs. *Physical Review Letters*, 25(2):84, 1970.

[20] David Fattal, Kyo Inoue, Jelena Vučković, Charles Santori, Glenn S Solomon, and Yoshihisa Yamamoto. Entanglement formation and violation of bell's inequality with a semiconductor single photon source. *Physical review letters*, 92(3):037903, 2004.

[21] Ivan Marcikic, Hugues de Riedmatten, Wolfgang Tittel, Valerio Scarani, Hugo Zbinden, and Nicolas Gisin. Time-bin entangled qubits for quantum communication created by femtosecond pulses. *Physical Review A*, 66(6):062308, 2002.

[22] Cheng-Zhi Peng, Tao Yang, Xiao-Hui Bao, Xian-Min Jin, Fa-Yong Feng, Bin Yang, Jian Yang, Juan Yin, Qiang Zhang, Nan Li, et al. Experimental free-space distribution of entangled photon pairs over a noisy ground atmosphere of 13km. *arXiv preprint quant-ph/0412218*, 2004.

[23] Xuan Han, Hai-Lin Yong, Ping Xu, Kui-Xing Yang, Shuang-Lin Li, Wei-Yang Wang, Hua-Jian Xue, Feng-Zhi Li, Ji-Gang Ren, Cheng-Zhi Peng, and Jian-Wei Pan. Polarization design for ground-to-satellite quantum entanglement distribution. *Opt. Express*, 28(1):369–378, Jan 2020.

[24] Cristian Bonato, Markus Aspelmeyer, Thomas Jennewein, Claudio Pernechele, Paolo Villoresi, and Anton Zeilinger. Influence of satellite motion on polarization qubits in a space-earth quantum communication link. *Opt. Express*, 14(21):10050–10059, Oct 2006.

[25] Vladimir B Braginsky, Vladimir Borisovich Braginskiĭ, and Farid Ya Khalili. *Quantum measurement*. Cambridge University Press, 1995.

[26] Sen Yang, Ya Wang, DD Bhaktavatsala Rao, Thai Hien Tran, Ali S Momenzadeh, M Markham, DJ Twitchen, Ping Wang, Wen Yang, Rainer Stöhr, et al. High-fidelity transfer and storage of photon states in a single nuclear spin. *Nature Photonics*, 10(8):507–511, 2016.

[27] Haruka Tanji, Saikat Ghosh, Jonathan Simon, Benjamin Bloom, and Vladan Vuletić. Heralded single-magnon quantum memory for photon polarization states. *Phys. Rev. Lett.*, 103:043601, Jul 2009.

[28] Nuala Timoney, Imam Usmani, Pierre Jobez, Mikael Afzelius, and Nicolas Gisin. Single-photon-level optical storage in a solid-state spin-wave memory. *Physical Review A*, 88(2):022324, 2013.

[29] CT Nguyen, DD Sukachev, MK Bhaskar, B Machielse, DS Levonian, EN Knall, P Stroganov, R Riedinger, H Park, M Lončar, et al. Quantum network nodes based on diamond qubits with an efficient nanophotonic interface. *Physical review letters*, 123(18):183602, 2019.

[30] Marek Zukowski, Anton Zeilinger, Michael A Horne, and Aarthur K Ekert. " event-ready-detectors" bell experiment via entanglement swapping. *Physical Review Letters*, 71(26), 1993.

[31] Carsten Schuck, Gerhard Huber, Christian Kurtsiefer, and Harald Weinfurter. Complete deterministic linear optics bell state analysis. *Phys. Rev. Lett.*, 96:190501, May 2006.

[32] John Calsamiglia and Norbert Lütkenhaus. Maximum efficiency of a linear-optical bell-state analyzer. *Applied Physics B*, 72(1):67–71, 2001.

[33] Ming Li, Pengfei Lu, Zhongyuan Yu, Yumin Liu, Lidong Zhang, and Chuanghua Yang. General model on polarization compensation in satellite-to-ground quantum communication. *Optical Engineering*, 52(4):045001, 2013.

[34] Ronald J Boain. Ab-cs of sun-synchronous orbit mission design. 2004.

[35] Hamid Hemmati. *Near-earth laser communications*. CRC press, 2020.

[36] Sidney A. Self. Focusing of spherical gaussian beams. *Appl. Opt.*, 22(5):658–661, Mar 1983.

[37] LC Andrews, RL Phillips, and PT Yu. Optical scintillations and fade statistics for a satellite-communication system. *applied optics*, 34(33):7742–7751, 1995.

[38] Ziqing Wang, Robert Malaney, and Jonathan Green. Satellite-based entanglement distribution using orbital angular momentum of light. In *2020 IEEE International Conference on Communications Workshops (ICC Workshops)*, pages 1–6, 2020.

[39] Gang Sun, Weng Ning-Quan, Xiao Li-Ming, and Yi Wu. Profile and character of atmospheric structure constant of refractive index c n 2. *Atmospheric and Oceanic Science Letters*, 5(3), 2012.

[40] Bernard J Klein and John J Degnan. Optical antenna gain. 1: Transmitting antennas. *Applied optics*, 13(9):2134–2141, 1974.

[41] Tom Vergoossen, Sergio Loarte, Robert Bedington, Hans Kuiper, and Alexander Ling. Modelling of satellite constellations for trusted node qkd networks. *Acta Astronautica*, 173:164–171, 2020.

[42] Juan Yin, Yuan Cao, Yu-Huai Li, Sheng-Kai Liao, Liang Zhang, Ji-Gang Ren, Wen-Qi Cai, Wei-Yue Liu, Bo Li, Hui Dai, et al. Satellite-based entanglement distribution over 1200 kilometers. *Science*, 356(6343):1140–1144, 2017.

[43] Juan Yin, Yu-Huai Li, Sheng-Kai Liao, Meng Yang, Yuan Cao, Liang Zhang, Ji-Gang Ren, Wen-Qi Cai, Wei-Yue Liu, Shuang-Lin Li, et al. Entanglement-based secure quantum cryptography over 1,120 kilometres. *Nature*, 582(7813):501–505, 2020.

[44] Adrien Dousse, Jan Suffczyński, Alexios Beveratos, Olivier Krebs, Aristide Lemaitre, Isabelle Sagnes, Jacqueline Bloch, Paul Voisin, and Pascale Senellart. Ultrabright source of entangled photon pairs. *Nature*, 466(7303):217–220, 2010.

[45] Albrecht Haase, Nicolas Piro, Jürgen Eschner, and Morgan W. Mitchell. Tunable narrowband entangled photon pair source for resonant single-photon single-atom interaction. *Opt. Lett.*, 34(1):55–57, Jan 2009.

[46] J Nunn, NK Langford, WS Kolthammer, TFM Champion, MR Sprague, PS Michelberger, X-M Jin, DG England, and IA Walmsley. Enhancing multiphoton rates with quantum memories. *Physical review letters*, 110(13):133601, 2013.

[47] Mikael Afzelius, Imam Usmani, Atia Amari, Björn Lauritzen, Andreas Walther, Christoph Simon, Nicolas Sangouard, Jiří Minář, Hugues De Riedmatten, Nicolas Gisin, et al. Demonstration of atomic frequency comb memory for light with spin-wave storage. *Physical review letters*, 104(4):040503, 2010.

[48] Dong-Sheng Ding. Raman quantum memory of photonic polarized entanglement. In *Broad Bandwidth and High Dimensional Quantum Memory Based on Atomic Ensembles*, pages 91–107. Springer, 2018.

[49] K. Surmacz, J. Nunn, K. Reim, K. C. Lee, V. O. Lorenz, B. Sussman, I. A. Walmsley, and D. Jaksch. Efficient spatially resolved multimode quantum memory. *Phys. Rev. A*, 78:033806, Sep 2008.

[50] Qing-Lin Wu, Naoto Namekata, and Shuichiro Inoue. High-fidelity entanglement swapping at telecommunication wavelengths. *Journal of Physics B: Atomic, Molecular and Optical Physics*, 46(23):235503, 2013.

[51] CCSDS Green Book. Real-time weather and atmospheric characterization data. *Informational Report, CCSDS*, 2017.